From the Division of Medical Imaging and Technology
Department of Clinical Science, Intervention and Technology
Karolinska Institutet, Stockholm, Sweden

# CHARACTERIZATION OF THE BOLD SIGNAL IN FUNCTIONAL MRI

Tomas Jonsson


Karolinska Institutet

Stockholm 2012

Published by Karolinska Institutet. Printed by Universitetsservice US-AB


ISBN 978-91-7457-627-6

*To Elina and Annelie*

# Abstract

In the last two decades, functional magnetic resonance imaging (fMRI) has become an important and widely used imaging technique for functional brain mapping. However, blood oxygen level dependent (BOLD) technique is quite insensitive and task invoked BOLD signal change at 3T is typically in the order of a few percent. Furthermore, the coupling between BOLD signal changes and neuronal activities is quite complicated, involving a cascade of events remaining poorly understood even today. In this thesis, some of the basic characteristics of the BOLD signal are investigated. Better understanding of the BOLD signal characteristics can be beneficial for the design of BOLD fMRI experiment aimed to improve the time efficiency. It can also provide guidelines for developing fMRI data processing strategies.

In study I and II, a single-shot dual-echo spiral acquisition technique was used for characterizing the $T_2$* changes associated with motor activation task. In **study I**, the optimal strategy for head motion correction was investigated. Based on the improvement in the detection of brain activation, the best strategy is to perform the head motion correction using the imaging data from the second echo and then apply the derived motion correction parameters to the first echo, instead of conducting motion correction of the individual echoes independently. In **study II**, several aspects of brain mapping methods based on $T_2$*-weighted imaging and $T_2$* ($R_2$*=1/$T_2$*) mapping were quantitatively compared, including the detected activation volume, functional contrast, signal-to-noise ratio, and contrast-to-noise ratio. fMRI studies based $T_2$* mapping have the following potential advantages: maximum functional contrast, independence of echo time; and reduced inflow effects. The sensitivity for brain activation detection is significantly correlated with the contrast-to-noise ratio, which is determined by both the signal-to-noise ratio and functional contrast.

In **study III**, the hemodynamic responses to functional activation were characterized using $T_2$*-weighted BOLD imaging, arterial spin labeling, and bolus tracking of MRI contrast agent. In addition to the BOLD signal change, the relative cerebral blood flow and cerebral blood volume associated with brain activation were independently determined.

In **study IV**, the characteristics of the global signal in resting-state fMRI were investigated. It was found that the global signal time courses and regional contributions differ individually. However, after removing the contribution from the cerebral spinal fluid, a consistent brain network responsible for the remaining global signal changes was identified. The involved brain regions include: posterior cingulate cortex, precuneus, superior temporal gyrus, medial frontal gyrus and the cerebellar vermis, which is likely to be related to the perception and cognitive processes of the brain occurred in the specific environments during resting-state fMRI.

# List of publications

This doctoral thesis is based on the following publications, referred to in the text by their Roman numerals.

I. **An image registration strategy for multi-echo fMRI**
**T. Jonsson**, A.B.A. Wennerberg, H. Forssberg, G.H. Glover, T-Q. Li
J Magnetic Resonance Imaging, 1999, 10, 154-158

II. **A comparative fMRI study: $T_2$*-weighted imaging versus $R_2$* mapping**
A.B.A Wennerberg, **T. Jonsson**, H. Forssberg, T-Q. Li
NMR in Biomedicine, 2001, 14, 41-47

III. **Assessment of hemodynamic response during focal neural activity in human using bolus tracking, arterial spin labeling and BOLD techniques**
T-Q. Li, T. Neumann Haefelin, B. Chan, A. Kastrup, **T. Jonsson**, G. H. Glover, M. E. Mosely
NeuroImage, 2000, 12, 442-451

IV. **The global signal of resting-state BOLD fMRI and associated brain network**
**T. Jonsson**, H. Fischer, A. Rieckmann, T-Q. Li
manuscript

# List of Additional Publications

Howner K; Fischer H; Dierks T; Federspiel A; Wahlund L-O; **Jonsson T**; Kristoffersen Wiberg M; Kristiansson M. Brain processing of fearful facial expression in mentally disordered offenders. Journal of Behavioral and Brain Science. 2011 Aug; Vol 1 (3): pp 115-123.

Petkova, VI; Bjornsdotter, M; Gentile, G; **Jonsson, T**; Li, TQ; Ehrsson, HH
From Part- to Whole-Body Ownership in the Multisensory Brain
Current biology 2011 Pages 1118-1122 Volume 21 Issue 13

Lindholm Terri L; Botes Lisa; Engman Eva-Lena; **Jonsson T** et al. Parallel imaging: is GRAPPA a useful acquisition tool for MR imaging intended for volumetric brain analysis? Source: BMC medical imaging 2009 Volume: 9

Bergfeldt U; **Jonsson T**; Bergfeldt L; Julin P. Central nervous system plasticity and functional effects in stroke patients receiving comprehensive focal spasticity management – an fMRI study. PhD Thesis 2009, ISBN 978-91-7409-523-4

Bergfeldt U; **Jonsson T**; Julin P.Atlas based analysis of single subject fMRI central nervous system activity during a hand motor task – a validity and reliability study in healthy individuals. PhD Thesis 2009, ISBN 978-91-7409-523-4

Wahlund K; Fischer H; Dierks T; Wahlund LO; Wiberg MK; **Jonsson T**; Kristiansson M. Psychopathy and brain imaging--a literature review. With focus on functional magnetic resonance tomography. Lakartidningen. 2009 Feb 4-10;106(6):361-5. Review.

Vannini, P; Almkvist, O; Franck, A; **Jonsson, T**; Volpe, U; Wiberg, MK; Wahlund, LO; Dierks, T Task demand modulations of visuospatial processing measured with functional magnetic resonance imaging Neuroimage 2004 Pages 58-68 Volume 21 Issue 1

Huang, CR; Wahlund, LO; Almkvist, O; Elehu, D; Svensson, L; **Jonsson, T**; Winblad, B; Julin, P Voxel- and VOI-based analysis of SPECT CBF in relation to clinical and psychological heterogeneity of mild cognitive impairment Neuroimage 2003 Pages 1137-1144 Volume 19 Issue 3

# List of Abbreviations

| | |
|---|---|
| 2D | Two-dimentional |
| 3D | Three-dimentional |
| $B_0$ | Main static magnetic field |
| BOLD | Blood oxygen level dependent |
| BT | Bolus tracking |
| (r)CBF | (relative)Cerebral blood fluid |
| (r)CBV | (relative)Cerebral blood volume |
| CC | Correlation coefficient |
| $CMRO_2$ | Metabolic rate of oxygen consumption |
| CNR | Contrast-to-noise ratio |
| CSF | Cerebral spinal fluid |
| DMN | Default mode network |
| EEG | Electroencephalogram |
| EPI | Echo planar imaging |
| FAIR | Flow-sensitive alternating inversion recovery |
| FC | Functional contrast |
| FLASH | Fast low angle shot |
| fMRI | Functional MRI |
| M1 | Primary motor cortex |
| MFG | Medial frontal gyrus |
| MRI | Magnetic resonance imaging |
| MRS | Magnetic resonance spectroscopy |
| MTT | Mean transit time |
| LFP | Local field potential |
| NMR | Nuclear magnetic resonance |
| PCC | Posterior singulate cortex |
| PET | Positron emission tomography |
| $R_2$* | Relaxation rate |
| RF | Radio frequency |
| rs | Resting-state |
| RVT | Respiration volume per time |
| SD | Standard deviation |
| SMA | Supplementary motor area |
| SNR | Signal-to-noise ratio |
| $T_1$ | Longitudinal relaxation time constant |
| $T_2$ | Transversal relaxation time constant |
| $T_2$* | Transversal relaxation time constant for gradient echo |
| TE | Echo time |
| TR | Repetition time |
| V1 | Primary visual cortex |

# Contents

# 1 Introduction

## 1.1 Historic overview

The discoveries made by Paul Lauterbur and Peter Mansfield in the 1970's have made it possible to develop the modern magnetic resonance imaging (MRI) technique based on the nuclear magnetic resonance (NMR) phenomena.
MRI represents a great breakthrough in medical diagnostics and research. In 2003, Paul Lauterbur and Peter Mansfield were awarded the Nobel Prize in Physiology or Medicine for their achievements. NMR phenomena itself was discovered already in 1946 by Felix Bloch(Bloch et al., 1946) and Edward Purcell(Purcell et al., 1946), whom were also awarded with Nobel Prize in 1952. NMR spectroscopy has now become widely used to study the molecular structures of pure materials and the composition of mixtures. With Lauterbur and Mansfields contributions (along with many others) the applications of NMR migrated to the medical imaging field.

## 1.2 Basic physical principles of mri

Analogous to mass and charge, spin and associated angular momentum is a fundamental property of particles. The spin quantum number, *I,* of a nucleus depends on the nuclear species, and has been observed to follow the pattern in table 1.

**Table 1.** Nuclear spin quantum number I

| Mass Number | Atomic Number | Nuclear Spin (*I*) | Example |
|---|---|---|---|
| odd | even or odd | 1/2, 3/2, 5/2, ... | $I(^1H) = 1/2$ |
| even | even | 0 | $I(^{12}C) = 0$ |
| even | odd | 1, 2, 3, ... | $I(^2H) = 1$ |

The nuclear spin quantum number gives rise to nuclear spin angular momentum, which in turn gives rise to a nuclear magnetic moment. In the absence of external fields, there is no preferred orientation for a magnetic moment. In the presence of a magnetic field, however, the energy of a nuclear magnetic moment depends on its orientation relative to the field:

$$E = -\mu_z B_0$$

where $\mu_z$ is the z-component of the magnetic moment, which can only take the discrete values

$$\mu_z = \gamma \hbar m$$

where $\gamma$ is the gyromagnetic ratio, $\hbar$ is Plancks constant and m is dependent on the angular momentum vector **I** can take the values

$$m = -I, -I+1, \ldots, I-1, I$$

In the presence of an external magnetic field, different nuclear spin states have different energies. The energy is a minimum when the magnetic moment is aligned parallel to the magnetic field and a maximum when it is anti-parallel to the magnetic field. At thermal equilibrium, nuclear spins at different energy states will be distributed according to the Boltzmann distribution. In practice, the difference between nuclear spin energy levels in achievable fields is very small, implying that the spin population between the different energy states is only very slightly different and, therefore, the sensitivity of NMR spectroscopy is very low.

NMR spectroscopy is performed by inducing transition between adjacent nuclear spin energy states ($\Delta m_I = \pm 1$). The understanding of NMR can be achieved by considering the effect of applied magnetic fields on the nuclear magnetic moments in the system. Briefly, an NMR sample in a homogenous external magnetic field is disturbed from equilibrium by application of a variable transverse secondary magnetic field, and its response to the disturbance is recorded. That is, the time dependence of the return to equilibrium is measured, from which frequency spectrum is generated via a Fourier transform. A tremendous enhancement of signal-to-noise (SNR) , as well as the ability to carry out multiple-pulse experiments can be achieved by replacing the traditionally used slow, sweeping field with short, intense radio-frequency (RF) pulses. Richard R. Ernst was awarded 1991 year's Nobel Prize in chemistry for his major contribution in this area.

## 1.3 MRI pulse sequence and k-space concept

The human body is largely composed of water and each water molecule has two hydrogen nuclei or protons. Proton has the quantum number, I = ½, implying that the hydrogen nucleus spin can exist in two possible energy states. Like most MRI applications for medical diagnostic purpose, the studies involved in this thesis are solely based on the spin state transition of protons. Protons in different tissues return to their equilibrium state at different relaxation rates. Different tissue characteristics, including spin density, $T_1$ and $T_2$ relaxation times, self-diffusivity, flow, and spectral shifts can all be used to construct images of different contrasts.

In order to obtain the spatial information of the signal origin in 3D space, additional magnetic fields need to be applied during a MRI scan. These fields, generated by passing electric currents through gradient coils, make the magnetic field strength vary depending on the position within the main static magnetic field. Because this makes the frequency of released radiofrequency signal also dependent on its spatial origin in a predictable manner, the distribution of protons in the body can then be mathematically recovered from the recorded NMR signal, typically by the use of the inverse Fourier transform.

In practice, a computer program called MRI pulse sequence is used to control hardware aspects of the MRI measurement process. It preselects a set of defined RF and gradient pulses of different shapes and durations. The pulse sequence is usually repeated many

times during a scan, wherein the time interval between pulses and the amplitude and shape of the gradient waveforms will control NMR signal reception and affect the characteristics of the images. By changing the settings, not only images of different sizes and resolutions can be acquired, the tissue characteristics can also be used to create contrast between the different tissues.

Unlike CT, MRI uses RF and gradient pulses, which are not ionizing radiation. Therefore, MRI is generally considered non-invasive, very safe and can be repeated for many times. MRI has been used to image every part of the body, and is particularly useful for tissues with many hydrogen nuclei and little density contrast, such as the brain, which is the focus of this thesis.

For simplicity, MRI physicists use the k-space formalism to describe the different MRI data acquisition methods. The k-space concept was independently introduced in 1983 by Ljunggren(Ljunggren, 1983) and Twieg(Twieg, 1983). In its essence, k-space is the 2D or 3D Fourier transform of the measured MR image. Its complex values are sampled during an MRI scan, in a premeditated scheme controlled by the pulse sequence. In practice, k-space often refers to the time-domain raw data sampled from the digitized NMR signals before image reconstruction.

Typically, k-space has the same number of rows and columns as the final image and is filled with raw data during the scan, usually one line per repetition time (TR). However, in a single-shot scan, such as, echo-planar imaging (EPI), the entire k-space is filled rapidly with raw data acquired during a single TR. The middle of k-space (lower k-space) contains the signal to noise and contrast information for the image, while data close to the boundary of k-space (higher k-space) contain the information determining the image spatial details (resolution). This is the basis for many advanced scanning techniques, such as, variable density spiral and keyhole acquisitions, in which the central k-space is more frequently sampled than the outer k-space.

## 1.4 Blood oxygen level dependent contrast

The discovery of blood oxygen level dependent (BOLD) contrast in the early 90's opened up a new research field in neuroscience. Before the discovery of BOLD fMRI, neuroscientists mainly used electro-encephalogram (EEG) and positron emission tomography (PET) to study the brain functional networks and their organization. With EEG, the electrical potentials caused by neuronal firings can be detected with sensitive electrodes placed on the skull. The temporal resolution of EEG is excellent, but the anatomical precision is poor, especially for the deeper brain structures, such as the basal ganglia. With PET, a radioactive tracer (such as $O^{15}$ and $^{18}F$) is injected into a subject and is followed in the brain's metabolism pathways to reveal the locations of the activated neurons in response to a specific task. Such metabolic measurements can map the oxygen and glucose consumptions in the brain, and, therefore, the brain functional activities.

When Ogawa coined the BOLD expression 1990 in his studies of rats (Ogawa et al., 1990), a method to trace brain activity without an invasive tracer was born and made the exploration of the brain function much more accessible for the neuroscience community. The first BOLD fMRI studies in humans were published two years later (Bandettini et al., 1992, Kwong et al., 1992, Ogawa et al., 1992), and ever since then, the number of brain studies using BOLD contrast has grown exponentially.

The BOLD contrast is based on the fact that deoxyhemoglobin is slightly paramagnetic (Pauling and Coryell, 1936), while oxyhemoglobin is diamagnetic. Simply speaking, the mechanism behind the detection of BOLD signal change in response to a brain activation is due to the mismatch between cerebral metabolism rate of oxygen consumption ($CMRO_2$) and cerebral blood flow (CBF) supply. When the brain is activated, the neurons start firing more intensively and hence consume more oxygen, which is extracted from the capillaries in the brain parenchyma. At first thought, the concentration of deoxyhemoglobin should therefore increase in the venous vessels and an initial MRI signal decrease is expected, because a higher concentration of deoxyhemoglobin increases the disturbance of the local magnetic field and the MRI signal decays faster. However, this is not what has normally been observed. Instead, an increase of the MRI signal has been observed. The detailed physiological mechanisms behind such phenomena have not yet been fully understood. However, with independent measurements of CBF and CBV, it can be estimated that the increased supply of oxyhemoglobin to the activated brain area excesses the local oxygen consumption and the concentration of oxyhemoglobin in the venous vessels is actually increased. Hence, less disturbance of the local magnetic field gives rise to an invoked MRI signal increase in response to a brain activation.

## 1.5 BOLD fMRI pulse sequences

To detect the subtle changes in the local magnetic field, the MRI pulse sequences need to be sensitive to susceptibility induced magnetic field inhomogeneity. Typically, a gradient recalled echo (GRE) pulse sequence is used for BOLD fMRI, where no refocusing RF pulse is used, as in the spin echo (SE) pulse sequences. On the other hand, for more accurate determination of anatomical locations, the SE pulse sequence are preferred, since the local stationary field inhomogeneity caused by e.g. air cavities, implants and hemorrhage, can be mitigated by the refocusing RF pulse. In the early days of BOLD fMRI, the fast low angle shot magnetic resonance imaging (FLASH) pulse sequence was used to detect the brain activation. The disadvantage with the FLASH data acquisition method is its limited temporal resolution. It takes quite a long time (a few second) to complete a single image slice, because only one row of k-space data can be collected per TR.

### 1.5.1 Echo Planar Imaging (EPI)

The GRE EPI has become the golden standard pulse sequence for BOLD fMRI. As shown in figure 1, its appealing features include a very fast acquisition scheme and high sensitivity to local field inhomogeneity, implying high sensitivity to the BOLD contrast. Even though the technique was invented 1977, the hardware to perform the pulse sequence was not quite ready until the beginning of 1990's. The technique was not even included into the standard pulse sequence library on many clinical MRI scanners until the late 1990's. EPI data acquisition has not only high demands on the gradient strength and slew rate but also stringent requirements for the signal digitization system, because it requires accurate broadband data acquisition and the raw data for a whole image slice has to be sampled during a few tens of milliseconds within a single GRE signal decay.

Depending of the number of slices, a whol- brain can be collected with EPI within 2-3 seconds, which gives a reasonable temporal resolution for functional brain studies. The main shortcoming associated with EPI data acquisition method is its sensitivity to off-resonance artifacts including ghosting, signal dropout, and geometrical distortions. These off-resonance artifacts are largely due to the local magnetic field inhomogeneity caused by magnetic susceptibility differences in the brain and poor shimming of the magnetic field. By conducting higher order shimming, the overall inhomogeneity in the brain can be reduced, but the problems associated with susceptibility differences are more difficult to handle. Especially in the orbital frontal regions of the brain, severe image distortions and signal dropout caused by the air cavities in the sinuses and ear canals are quite common. With the advent of parallel acquisition techniques in last decade, the EPI image quality has been greatly improved.

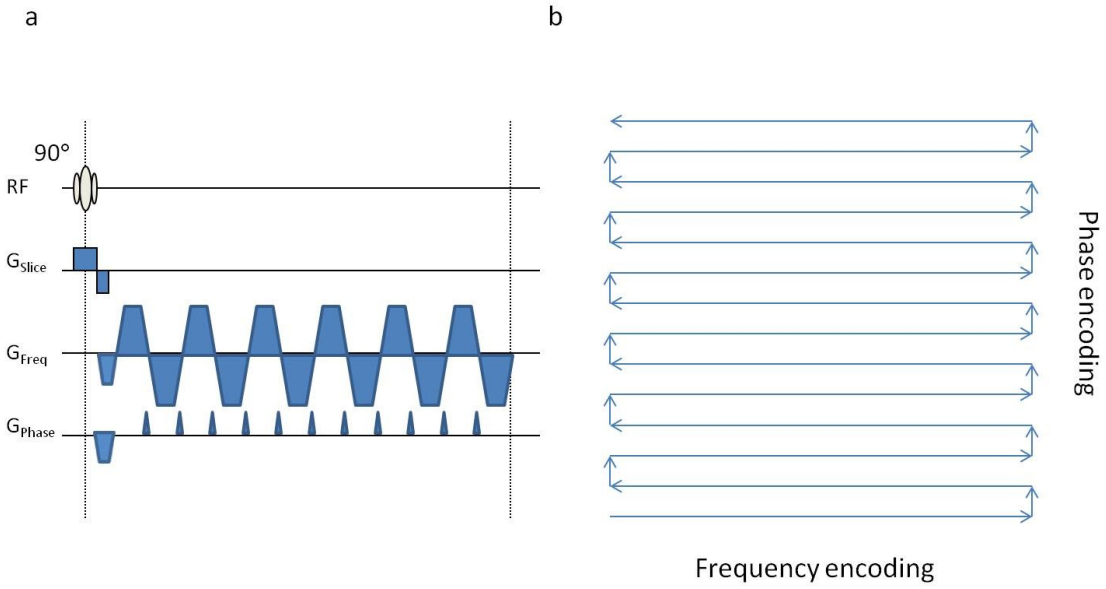


**Figure 1.** The schematic time schedule of a typical EPI sequence. (a) The timings of the slice selection, frequency, and phase-encoding gradient waveforms and slice selection RF pulse. (b) The k-space trajectory

### 1.5.2 Spiral pulse sequence

Like the EPI acquisition method, the data acquisition with spiral pulse sequence can also be completed with single-shot. This means that the entire k-space can be sampled within a single TR. With the spiral pulse sequence, the k-space sampling starts normally at the center and then continuously spirals out in a spiral trajectory to cover the entire k-space (see figure 2). The main advantages associated with the spiral acquisition method include starting the center k-space sampling at the beginning of the acquisition while the signal is strong, high time efficiency, less stringent demand on the gradient hardware duet to the lack of phase-encoding, and robustness against motion artifacts. Modified spiral acquisition methods based on the combinations of spiral-in and spiral-out readouts have also been demonstrated to be robust against susceptibility artifacts. Since the spiral readout does not follow regular Cartesian trajectory, gridding procedure is required for the image reconstruction and the regridding procedure is usually carried out off-line. Approximations used in the gridding algorithm and other off-resonance effects can all contribute to blurring artifacts in the reconstructed spiral images. Because of the robustness of the spiral acquisition method, most of the studies (I-III) included in the thesis were based on the spiral pulse sequence.

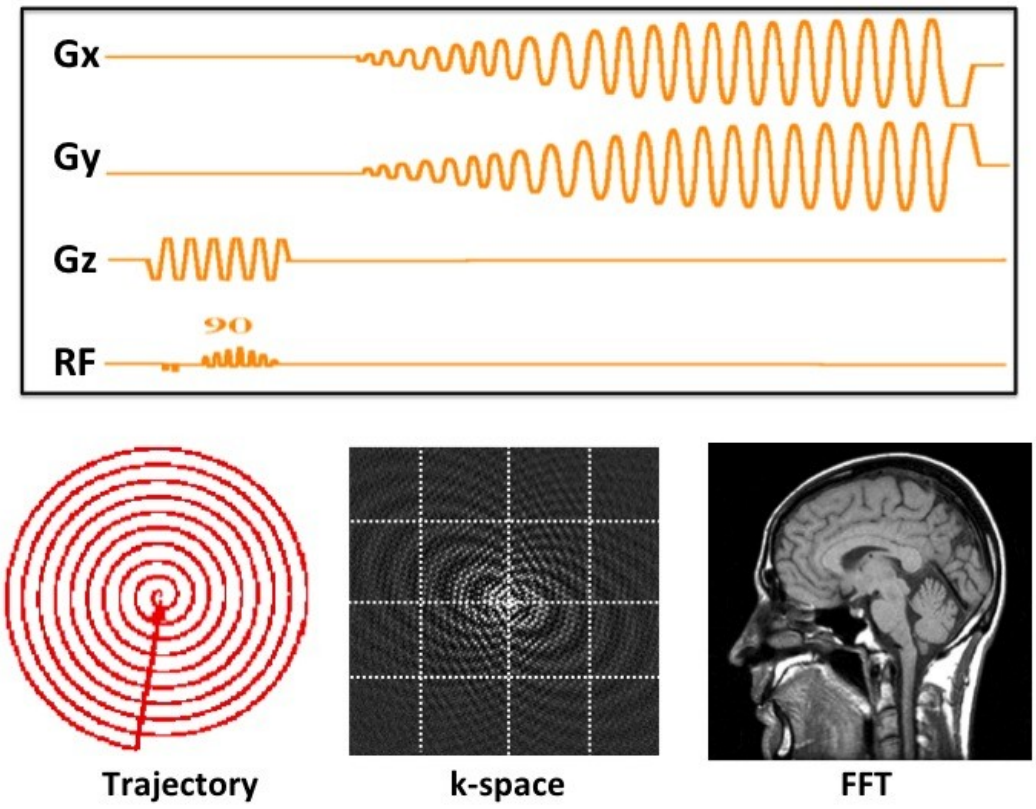


**Figure 2.** The spiral sequence is shown. Upper figure shows the gradient time schedule. In the lower left image the k-space trajectory. The lower middle image shows the real k-space and the lower right image shows the final image after Fourier transformation.

### 1.5.3 Anatomical references

Since the pulse sequences discussed above are meant for rapid sampling of the functional MRI data and offer relatively low spatial resolution. In fMRI studies, high-resolution anatomical reference images are usually acquired to cover the brain areas of interest. With registration software, the low resolution fMRI data can be registered onto the anatomical reference dataset for better localization of the activated brain areas. Furthermore, the high-resolution anatomical reference scan can also facilitate the inter-subject comparison of the fMRI data by improving the registration quality of the individual brain data with the standard brain template. A $T_1$-weighted 3D pulse sequence is usually preferred, but $T_2$-weighted pulse sequences can also be used, as done in study I and II.

## 1.6 Some characteristics of the BOLD signal

fMRI BOLD signal has its unique characteristics. As mentioned above, it can be detected non-invasively with relative high-resolution at any given specific brain region. However, it has poor sensitivity, low temporal resolution, and provides only an indirect measure of neuronal activity. A better understanding of its pros and cons can be very useful for the fMRI experimental design in order to maximize its strengths and minimize its weaknesses.

### 1.6.1 TE dependence

As has previously been shown, the sensitivity of BOLD signal is TE dependant (Bandettini et al., 1994, Jonsson, 1997). The functional contrast, that is the signal difference between activation and reference states, has an optimum. It has been experimentally and theorectially demonstrated that the maximum functional contrast can be achieved at $TE \approx T2^*$. This is also illustrated in figure 3, where the MRI signal decays for typical T2* values of activation and resting state at 1.5 T are plotted.

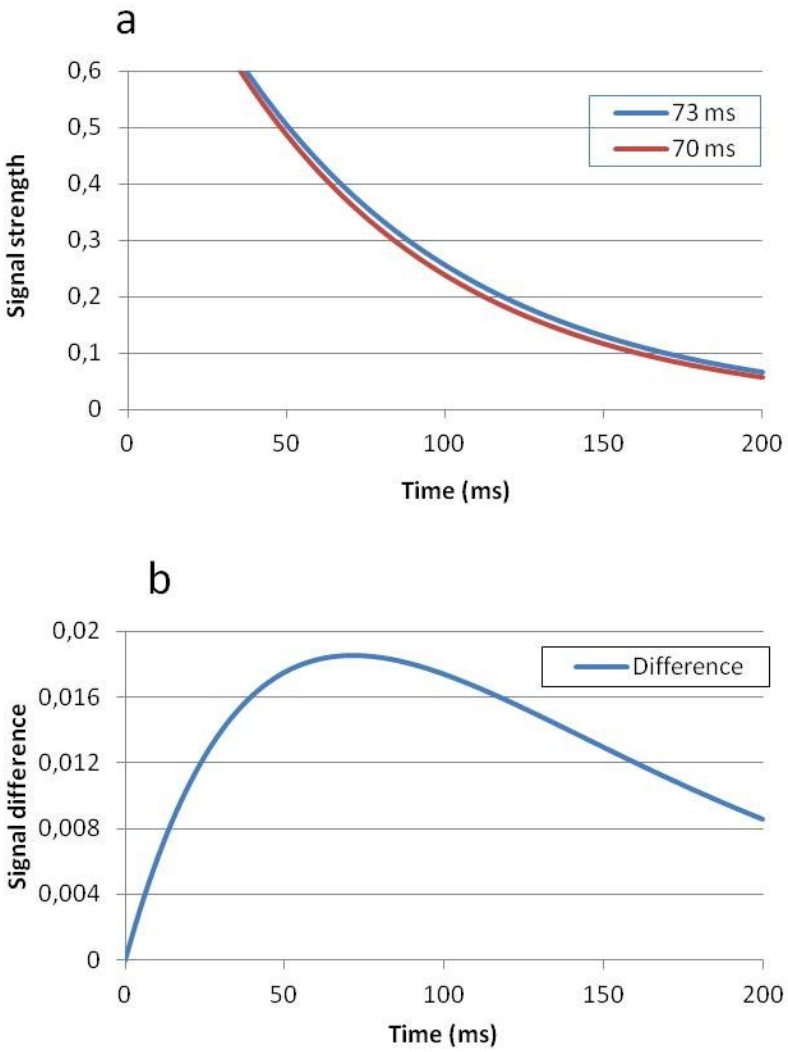


**Figure 3.** The TE dependence of fMRI BOLD signal. (a) signal decays for two typical $T_2$* values of brain tissue at 1.5 T, 73 ms for activation and 70 ms for resting state, respectively. (b) the signal difference between the two decay curves as a function of TE. The maximum difference appears around TE ≈ $T_2$*.

By assuming exponential decay, it can be mathematically shown that the maximum difference between two GRE signals of differenct $T_2$* values can be achieved when

$$TE_{opt} = \frac{ln[R_2^*(a)] - \ln[R_2^*(r)]}{R_2^*(a) - R_2^*(r)}$$

where $R_2$* is $1/T_2$* and $a$ and $r$ is the $R_2$* value for activation and resting states respectively.

Since $T_2$* is dependent on the main magnetic field strength and decreases with $B_0$, the optimal TE for BOLD fMRI studies is different at different field strength and the

estimate of $T_2$* should be carried out adequately in order to optimize the sensitivity of the BOLD fMRI measurements.

### 1.6.2 Temporal characteristics of the BOLD signal

The temporal behavior of the BOLD signal is determined by the hemodynamic response involving the associated CBF and CBV changes. Figure 4 shows a schematic representation of the hemodynamic response function to a brief stimulus applied at time t = 0 sec.

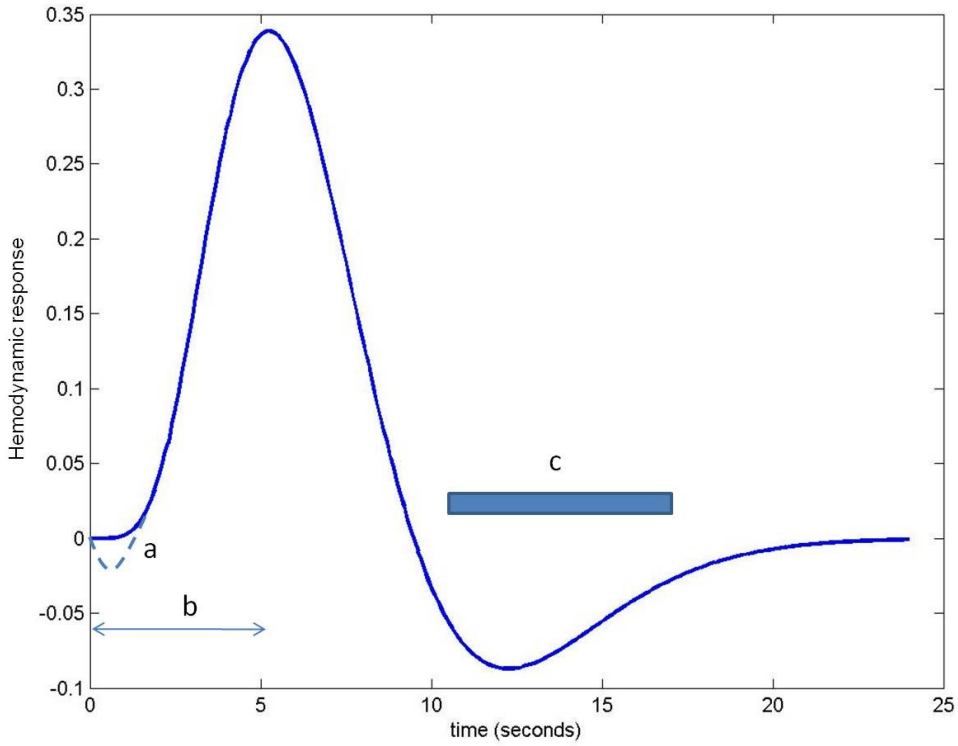


**Figure 4**. A schematic diagram of the hemodynamic response function. (a) is the initial dip immediately after the stimulus, (b) is the time needed for the BOLD signal to reach its maximum, and (c) illustrate the post-stimulus undershoot.

#### *1.6.2.1 The initial dip*

The initial dip, or the so-called fast response, is usually not seen at magnetic field strengths < 3 T which made it a bit controversial when it was first reported (Ernst and Hennig, 1994, Menon et al., 1995), since most fMRI sites had only 1.5 T scanners at that time. This effect is now believed to represent the increased demand of oxygen from the stimulated neurons before the start of blood flow increase, which causes an increased concentration of deoxyhemoglobin in the blood, and gives rise to a negative BOLD response. Its typical magnitude is about 0.5-1 % lasting up to 1 second. This effect vanishes when the blood flow response starts due to the increased demand of

oxygen. The precise physiological mechanisms behind the increased blood flow supply are still not very clear at the present time.

#### *1.6.2.2 BOLD signal maximum*

The time that takes for the BOLD signal to reach its maximum in response to a brief stimulus has been reported to be between 4-8 seconds. For a sustained activation task, lasting for several seconds, an over-shoot may be observed at the beginning of the BOLD response. This overshoot can be explained by the slower response of the cerebral blood volume. The magnitude of the maximum is usually in the order of a few percent depending on the types of used stimuli. The BOLD signal change may also differ individually.

#### *1.6.2.3 The Post-stimuli undershoot*

After the stimulus has ceased the BOLD signal returns to the baseline, but a post stimulus undershoot can occur, which delays the return to baseline with several seconds. Even if the blood oxygenation level and the cerebral blood flow return quickly back to the baseline levels, the CBV lags with a much slower transient response (Buxton et al., 1998).

### 1.6.3 Noise sources in the BOLD signal

Accurate detection of the BOLD signal is hampered by its low sensitivity and various noise sources in BOLD fMRI measurements. The signal noise can be commonly divided into thermal and non-thermal noise. The thermal noise is inherent to the MRI imaging process and originates from the subject itself and the electrical circuits and components in which the MRI signal is induced and transported. This kind of noise, also called “white noise”, is hard to remove afterwards, and can be reduced by choosing high end equipment, such as high field scanners and phased array coils with short cables. The non-thermal noise consists of a variety of noise sources, such as physiological (cardiac and respiration) noise, head movements, spontaneous neuronal activation and linear drifts in the scanner electronics (Kruger and Glover, 2001, Kruger et al., 2001). The non-thermal noise also has components that scale with the signal SNR and the physiological noise can be the dominating source at higher magnetic field strength(Triantafyllou et al., 2005).

In every major software package for fMRI data analysis, both motion correction of the head movements and linear de-trending of the data are included as standard preprocessing steps. To reduce the influence of the physiological noise, several correction methods have been developed. The simplest approach is to perform a high pass filtering, where slowly varying frequencies are filtered out from the data set. Since the typical TR used of whole-brain fMRI scans is in the order of 2-3 seconds, the physiological activities can be under-sampled and appears as aliased signals with much lower frequency. When auxiliary physiological data, such as the cardiac and respiratory

waveforms, are recorded, more sophisticated approaches can be used to retrospectively remove the physiological noise (Hu et al., 1995, Glover et al., 2000). Recently, regression analysis based noise reduction has become quite attractive for fMRI studies, as high field MRI scanners are more accessible and physiological noise reduction becomes a very relevant issue. The key point for regression analysis is to construct creative regressors effective for noise reduction (de Zwart et al., 2008).

#### *1.6.3.1 Noise reduction in resting-state fMRI*

The resting brain is not resting at all. Resting-state fMRI investigations have revealed coherent intrinsic activity identified by mapping patterns of slow temporal coherence (< 0.1 Hz) of signal fluctuations between brain regions, which is often referred to as functional connectivity (Biswal et al., 1995, Raichle et al., 2001, Fransson, 2005, Biswal et al., 2010). A number of co-activating functional systems have been found consistently across subjects (Beckmann et al., 2005, Damoiseaux et al., 2006, Öberg et al., 2011) covering brain regions known to be involved in motor function, visual processing, executive function, auditory processing, memory and the so called default-mode network. To enhance these networks and suppress the background noise, several noise reduction methods have been developed. Much attention has been given to reducing the physiological noise components which have been aliased into the frequency range of interest (< 0.1 Hz). Studies have shown that spontaneous fluctuations in end-tidal $CO_2$ correlate significantly with resting-state fMRI time series (Wise et al., 2004, Chang and Glover, 2009b), which implies that not only the respiratory cycle but also the respiratory volume variation influences the resting-state fMRI signal. Several studies have addressed these issues and suggest correction methods for both respiratory (Birn et al., 2006) and cardiac (Shmueli et al., 2007, Chang et al., 2009, van Houdt et al., 2010) variations.

In most resting-state fMRI studies, the average time-course from all voxels in the brain, the global signal, is removed from the data to further enhance the detection of the local neuronal networks. This is justified by assuming that the global signal contains signal from non-neuronal sources, such as instrumental noise, physiological noise, CSF and white matter. This has partly been verified and there is a significant correspondence between the global signal and cardiac and respiratory activities (Birn et al., 2008, Chang and Glover, 2009a). One problem with the removal of the global signal from the resting-state fMRI data is the contingency if the regression introduces anti-correlated networks (Chang and Glover, 2009a, Fox et al., 2009, Murphy et al., 2009, Cole et al., 2010), especially the default-mode network. A solution for this problem could be a combined regression of the white matter average signal, CSF average signal and motion correction parameters, which provides an effective approach for dealing with global correlations. This has also the advantage of reducing the risk of introducing “fictitious” negative correlations into the datasets (Giove et al., 2009).

# 2 Aims of the thesis

In this thesis, some of the basic characteristics of the BOLD signal are investigated. Better understanding of the BOLD signal characteristics can be beneficial for the optimization of the BOLD fMRI experiment design aimed to improve the time efficiency. It can also provide guidelines for developing fMRI data processing strategy.

The specific aims for the individual studies are the following:

**Study I** – To use a single-shot dual-echo spiral pulse sequence for fMRI study and develop an optimal strategy for image registration of the dual-echo fMRI data.

**Study II** - To systematically compare BOLD fMRI results based on $T_2$* mapping and $T_2$*-weighted imaging in terms of the detected activation volume, signal-to-noise ratio (SNR), the functional contrast (FC), and functional contrast to noise ratio (CNR). To characterize the T2* changes induced by brain activation at 1.5T.

**Study III** – To use different MRI techniques including sequential bolus tracking measurements of a contrast agent, T2*-weighted imaging and arterial spin labeling for fMRI studies. To measure the CBF, CBV, and BOLD signal changes induced by motor and visual stimuli.

**Study IV** - To characterize the global signal changes in resting state fMRI measurements in normal volunteers. To identify the brain regions responsible for the generation of the global signal changes, and elucidate the possible underlying mechanisms.

# 3 Methods

## 3.1 Experimental setup

An overview of the hardware, data acquisition method, and scanning parameters used in the BOLD fMRI experiments are listed in table 2.

**Table 2.** The BOLD fMRI setups for the different studies.

| Study | Scanner | Sequence | TR/TE/$TE_2$ | Resolution ($mm^3$) | Stimuli | Subjects |
|---|---|---|---|---|---|---|
| **I & II** | GE Signa 1.5 T | Double echo Spiral | 3s/20ms/90ms | 1.7x1.7x5 | Motor | 6 |
| **III** | GE Signa 1.5 T | Spiral | 3s/45ms | 1.7x1.7x5 | Motor Visual | 8 |
| **IV** | Siemens Trio 3 T | EPI | 2.5s/35ms | 3x3x3 | Resting state | 71 |

### 3.1.1 Study I and II

Six healthy subjects were scanned. In study II, the subjects were scanned at least at three different occasions which produced a total of 19 datasets. The functional images were acquired in the motor areas of the brain, including motor cortex, premotor cortex and the supplemental motor area, SMA. A single-shot dual-echo spiral sequence (Li et al., 2006) with two different echo times, $TE_1$ = 20 ms and $TE_2$ = 90 ms was used for the fMRI data acquisition (see figure 5). The six volunteers performed a motor paradigm, in which they were instructed to do self-paced finger tapping with their right hand during 4 epochs of activation interleaved with 5 epochs of resting periods, to achieve robust motor activation in the brain. To reduce the motion artifacts in the images the volunteers' heads were immobilized with a bite bar.

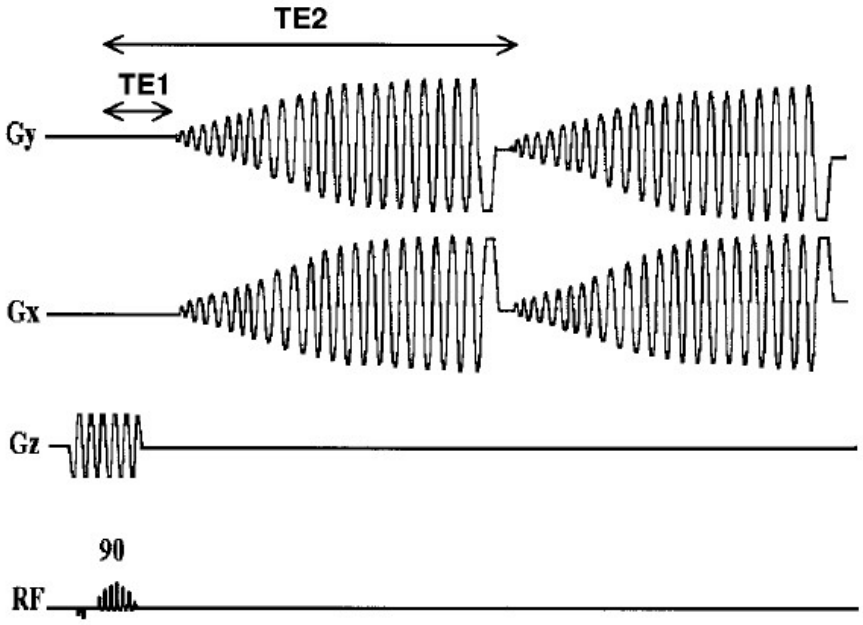


**Figure 5.** The pulse sequence used for the study plays out two successive spiral readouts after each excitation. The data acquisition for the first echo image starts at $TE_1$= 20 ms and the spiral readout lasts for 65.6 ms. The same readout waveforms were used for the acquisition of the second echo image with $TE_2$ = 90 ms.

### 3.1.2 Study III

In study III, the functional MRI data acquisition protocol consisted of four sessions: FAIR, BOLD and two bolus tracking measurements. Both motor and visual stimuli were used for obtaining the maximum information with only one bolus tracking (BT) experiment. Eight volunteers participated in the study. The motor stimulus was a self-paced finger tapping task, and the visual stimulus was a flickering checkerboard pattern presented for each subject on a screen inside the MRI scanner bore, with an 8 Hz flickering frequency. The FAIR pulse sequence measures the rCBF changes in the brain, while the T2*-weighted GRE measurement provides the change in the BOLD signal in the activated brain regions. The BT experiment consisted of one bolus injection without activation and a second injection with brain activation tasks 10 min after the initial injection. With these BT measurements, the rCBF and rCBV changes induced by the brain activation tasks can be estimated. For the $T_1$ mapping needed for the FAIR measurements, a Look-Locker pulse sequence was used.

.

### 3.1.3 Study IV

A total of 71 volunteers participated in the study, and a total of 108 resting-state (rs) fMRI data sets were collected, lasting 10 minutes. For 19 of the subjects, also physiological data was recorded (respiration and cardiac waveforms). Six subjects were scanned with a prolonged rs-fMRI measurement, lasting for 42 minutes. A phantom was also scanned during 50 minutes for control measurements at three times. The fMRI sequence was a standard EPI acquisition with a TR of 2.5 sec and a TE of 35 ms. The in plane resolution was 3x3x3 $mm^3$.

## 3.2 Data preprocessing

The preprocessing procedure involves a number of steps where the data sets are prepared for the detection of brain functional activation. Since the BOLD signal amplitude is only a few percent of the total signal, the preprocessing procedure can be crucial for a successful detection of these tiny BOLD signal changes.

### 3.2.1 Study I and II

For study I, the question was how to optimize the preprocessing steps for achieving the most sensitive detection of the BOLD signal. In fMRI studies with sing-shot data acquisiton, it is a standard procedure to perform rigid body image registration in order to correct for the small head motions that occur involuntarily during the scans. For fMRI datasets acquired with dual-echo pulse sequence, there was no motion correction procedure available at the time when the study was carried out. We tested two different approaches; in order to take into account the different contrast in the two different echoes, motion registration was first conducted independently with the individual echo datasets, at $TE_1$ and $TE_2$, This procedure was named as SepReg. The second approach was to do the motion correction with the data acquired at the late echo at $TE_2$ and then apply the motion correction parameters for in-plane translational and rotation motions to the first echo data at $TE_1$. This procedure was labeled as SigReg. After image registration, a $T_2$* map was calculated from each dual echo image pair on a pixel-by-pixel basis using the signal intensities from the $T_2$*-weighted images at $TE_1$ and $TE_2$. Assuming that $T_2$*-relaxation obeys a mono-exponential function $T_2$* is given by

$$\frac{1}{T_2^*} = \frac{ln(S_{TE1}) - ln(S_{TE2})}{TE_2 - TE_1}$$

where $S_{TE1}$ and $S_{TE2}$ are the signal intensities of the $T_2$* - weighted images at $TE_1$ and $TE_2$, respectively.
In study II, we used the most efficient motion correction strategy, SigReg, derived from study I to register the fMRI data before further analysis.

### 3.2.2 Study III

All data sets were motion corrected with the auxiliary program imreg from the AFNI software package(Cox, 1996).

The FAIR images were calculated by magnitude subtraction of the nonselective inverted images from the selective inverted images (Li *et al.,* 1999a, b). The CBF quantification from the FAIR measurements was based on the perfusion model of Detre *(Detre et al., 1992)*. The baseline data collected prior to the onset of the sustained activation was used as a reference to calculate the relative CBF changes induced by the activation.

Since each FAIR image requires a pair of images with selective and nonselective inversion, the temporal resolution of the FAIR data was 6 s with a TR of 3 s.

For the bolus tracking measurements, the image data was processed using the deconvolution algorithm described by Østergaard et al (Ostergaard et al., 1996a, Ostergaard et al., 1996b). This resulted in rCBF and rCBV maps for both the resting and activation states. Since the time interval between the two successive BT measurements is too short for the contrast agent to be cleared out from the vascular system, an effect of the residual contrast agent from the first injection can be detected. This has carefully been corrected by using a scheme based on the assumption that non-activated regions should have the same regional CBF and CBV values in the two successive BT measurements.

### 3.2.3 Study IV

All the functional image data was preprocessed before the statistical analysis in the same way:

- Exclusion of the first 10 time frames to ensure that the BOLD fMRI signal reached the steady state.
- Head motion correction. Two data sets were excluded because of too much motion.
- Creation of a whole brain mask, for excluding non-brain tissue.
- Registration to a standard brain atlas in Talairach-Tournoux space
- A global-signal mask was created of the registered brain volumes
- Spike removal and low pass filtering at a threshold of 0.1 Hz. This step also included the linear de-trending to remove first-order baseline drifts.
- Voxel-wise high order de-trending using least-square curve fitting and removal of polynomial trends.

For the 19 subjects with physiological recordings, the program RETROICOR(Glover et al., 2000) removed the cardiac and respiration waveforms from the data sets. To further study the impact of the different preprocessing steps, these data underwent three levels of regression analysis to remove non-neuronal signals. The levels consisted of:

1) Alignment parameters, cardiac rate, and RVT time course;
2) Alignment parameters and the average CSF time course;
3) Alignment parameters, cardiac rate, RVT, and the average CSF time course.

Here the alignment parameters are taken from the motion correction step, the cardiac rate is derived from the cardiac data, RVT is the respiratory volume per time derived from the respiration data and the CSF time course is the average time course taken from the functional data masked with a CSF template taken from standard tissue-type probability maps provided by the FSL group (www.fmrib.ox.ac.uk/fsl/fsl/list.html).

For the remaining subjects without physiological recordings, regression analysis was performed with alignment parameters and average CSF time course as regressors.

## 3.3 fMRI data analysis

### 3.3.1 Study I

The calculated T2* maps were statistically analyzed using the fMRI software AFNI(Cox, 1996) for functional activation detection. Statistical significance of the activation was assessed by cross-correlation thresholding and cluster analysis. An ideal boxcar reference waveform having a 30 second period of activation, assigned a value of 1, alternating with a 48 second period of rest, assigned a value of 0, was used. The same reference waveform was used for both original and registered data. Using a threshold correlation coefficient of at least 0.55 guaranteed that the significance *P* was less than 0.001, after including a multiple comparison correction. A minimum cluster size of 3 pixels was also adopted to produce the final activation maps, which further improves the statistical significance level of the detected activation. The total number of activated voxels was determined by counting the activated voxels in all the slices.

### 3.3.2 Study II

Based on the results from study I, we used the SigReg data set for further analysis. We also included the $T_2$*-weighted images at $TE_1$ and $TE_2$ for the statistical analysis. The $T_2$*-maps was converted to $R_2$*-maps by

$$R_2^* = \frac{1}{T_2^*}$$

These three types data were all analyzed using a student t-test with a t-score threshold of 3.2, which gave a significance of $p < 0.001$. To further reduce false positive results, the detected voxels were clustered with a minimum cluster size of 5 voxels. The mean time series from the remaining detected voxels from the motor cortex regions was extracted for the different data sets, and used for parameter comparison between the different methods. The total number of activated voxels was also counted.

Three different parameters were investigated: SNR, FC and CNR. The signal-to-noise ratio, SNR is given by

$$SNR = \frac{\bar{S}}{\sigma}$$

where S and σ are the mean signal intensity and the square root of the variance of the subtracted image between two consecutive time frames, respectively.

The functional contrast, FC, was estimated by using the following definition:

$$FC = \frac{|\Delta S|}{\bar{S}_{rest}} = \frac{|\bar{S}_{\mathrm{act}} - \bar{S}_{\mathrm{rest}}|}{\bar{S}_{rest}}$$

where the mean signal intensities in activation and resting states are represented by $\bar{S}_{act}$ and $\bar{S}_{rest}$.

Finally, the contrast to noise CNR was estimated by using the following relationship:

$$CNR = \frac{\Delta S}{\sigma} = SNR \cdot FC$$

### 3.3.3 Study III

The fMRI data analyses were performed differently depending on the different imaging data acquisiton methods that were used. The FAIR pulse sequence requires a pair of images, with and without selective inversion, and the temporal resolution was only half of the BOLD images, 6 sec and 3 sec respectively. The BOLD and FAIR data were analyzed similarly, with a student's t-test and the same t score threshold and cluster analysis. After including a multiple comparison correction, using a threshold *t* score > 3.2 guaranteed that the significance *P* was less than 0.001. A minimum cluster size of 5 pixels was also implemented to produce the final activation maps. The activation induced signal changes in the motor and visual cortexes for both the BOLD and the FAIR experiments were evaluated by analyzing the mean time courses of the voxels in the activated areas. The mean time series for further analysis was taken from the areas where both methods detected activation.

For the BT measurements, a correction for the remaining contrast agent in the second run was carried out throughout the brain. The corrected CBV and CBF maps for the resting and activation states were subtracted to reveal areas involved in the functional tasks using a threshold of 2 standard deviations above the mean of the subtracted images. The relative CBV and CBF changes associated with the functional activation were determined from the subtracted images as the mean values of the voxels that were activated in both BOLD and FAIR measurements.

### 3.3.4 Study IV

The global signal was calculated for each data set, using the brain mask which was created in the preprocessing step. A power spectrum for each subject's global signal was calculated. All voxels in the brain were cross correlated to the global signal time course. The calculated cross-correlation coefficients were converted into t-statistics of correlation. Maps were created showing the differences in cross-correlation coefficient between regression analyses with successive addition of regressors, which would reveal the anatomical locations responsible for the differences. To determine whether the anatomical locations responsible for the global signal changes were consistent across subjects, group maps of pooled **t**-statistics were created from the individual **t**-maps(Jansma et al., 2001). A voxel-based **t**-test was carried out to test whether the mean **t** value over all the subjects was significantly different from zero, using a pooled standard deviation over all voxels. The t-maps were then produced using a voxelwise t-score threshold of 3.2 and a minimum cluster size of 40 µl. The clusters which survived the **t**-score and cluster size thresholds were detected using the AFNI routine *3dclust*. The coordinates for the center of gravity of each cluster, along with its cluster size, average, and maximum correlation coefficient were extracted using the AFNI ROI utility programs.

# 4 Results

## 4.1 Study I

All the calculated data for the six subjects is summarized in table 3.
All subjects showed distinct activation in the primary sensorimotor cortex, as well in the supplementary motor area. For the motion corrected datasets, 4 of 6 subjects showed bilateral activation in the primary sensorimotor cortex as can be expected in this kind of stimuli. The number of activated voxels increased in both methods of motion correction for all subjects. The average increase was 13% for SepReg and 15% for SigReg method.

**Table 3.** Number of Activated Voxels and $T_2$* Values at Activated and Baseline States Results for Nonregistered (NotReg) and Registered Data (SepReg and SigReg)

| Data set | 1 | 2 | 3 | 4 | 5 | 6 | Mean |
|---|---|---|---|---|---|---|---|
| Activated voxels | | | | | | | |
| NotReg | 341 | 372 | 1595 | 367 | 326 | 338 | 556 |
| SepReg | 361 | 471 | 1799 | 407 | 366 | 365 | 628 |
| SigReg | 381 | 493 | 1811 | 417 | 371 | 360 | 639 |
| $T_2$* values for activated state in ms | | | | | | | |
| NotReg | 79.5±2.5 | 75.8±3.0 | 67.2±2.9 | 74.7±1.9 | 74.1±3.1 | 71.0±2.6 | 73.7±2.7 |
| SepReg | 78.8±2.3 | 77.7±2.8 | 66.7±2.5 | 75.2±1.6 | 73.4±3.0 | 69.3±2.4 | 73.5±2.4 |
| SigReg | 77.4±2.3 | 77.6±2.6 | 66.7±2.6 | 75.0±1.6 | 73.3±3.0 | 69.5±2.4 | 73.3±2.4 |
| $T_2$* values for resting state in ms | | | | | | | |
| NotReg | 75.1±2.7 | 71.0±2.5 | 64.3±2.5 | 70.7±2.3 | 70.3±2.4 | 67.8±2.0 | 69.9±2.4 |
| SepReg | 74.7±2.6 | 73.3±2.4 | 64.1±2.2 | 71.3±2.2 | 70.1±2.4 | 66.3±1.9 | 70.0±2.3 |
| SigReg | 73.3±2.5 | 73.2±2.3 | 64.1±2.2 | 71.1±2.2 | 70.0±2.4 | 66.5±1.9 | 69.7±2.3 |

The mean $T_2$* value was calculated from the activated voxels for the activation state and for the resting state. The mean values based on all subjects were 73.4 and 69.8 ms for the activation and resting states, respectively. The average $T_2$* value did not differ significantly between the non-registered datasets and the registered datasets , but the standard deviation decreased by 11 % when comparing the registered datasets with the unregistered datasets.

## 4.2 Study II

Both the $R_2$* maps and the $T_2$*-weighted images were analyzed for the detection of functional brain activation. Robust activation in the contralateral primary motor cortex and primary somatosensory cortex was detected in all datasets. An example activation map from one subject is shown in figure 6. The detected activation volume, FC, SNR and CNR were calculated for each data set. The activation volume demonstrated significant inter-subject variability but was relatively constant for the same subject measured at different occasions. A summary of the results is listed in table 4. The largest detected activation volume was found in echo 2 datasets. About 40 % more voxels was detected than the results from the datasets of $R_2$* maps, while the first echo detected only one third of the volume compared with the second echo datasets. The average functional contrast, FC, was 1.7 % for echo 1, 4.4 % for echo 2 and 6.2 % for the $R_2$* map. On the contrary, the signal-to-noise goes in the opposite direction. The average SNR values were 98, 42 and 32 for echo 1, echo 2 and $R_2$* map, respectively. For the contrast-to-noise, CNR, the highest value is found for the $R_2$* map at 1.95, followed by echo 2 at 1.87. Datasets from echo 1 has the lowest average CNR at 1.70. The calculated averaged $R_2$* values for the activation and the resting states were 13.21 $s^{-1}$ and 14.08 $s^{-1}$ respectively. These $R_2$* values correspond to the $T_2$* values of 75.7 ms for the activation state and 71.4 ms for the resting state, which are in good agreement with the results from the literature.

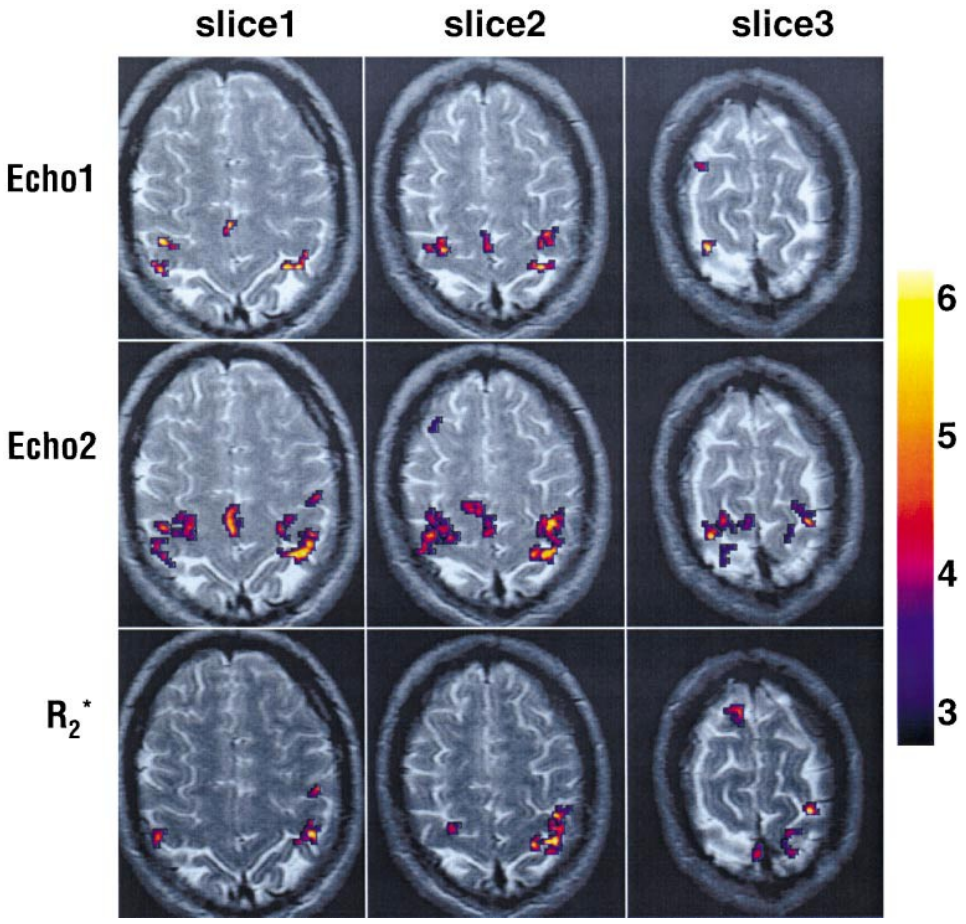


**Figure 6.** A typical set from one subject. The three slices cover the motor areas.

**Table 4**. Summary of the detected activation volume, functional contrast, signal-to-noise ratio for the first echo, second echo and $R_2$* parametric maps.

| | Echo 1 | | | | Echo 2 | | | | $R_2$* | | | |
|---|---|---|---|---|---|---|---|---|---|---|---|---|
| | Volume (voxels) | FC (%) | SNR | CNR | Volume (voxels) | FC (%) | SNR | CNR | Volume (voxels) | FC (%) | SNR | CNR |
| Mean | 296 | 1.7 | 98 | 1.70 | 818 | 4.4 | 42 | 1.87 | 581 | 6.2 | 32 | 1.95 |
| SD | 106 | 0.3 | 7 | 0.28 | 164 | 0.4 | 4 | 0.17 | 129 | 0.5 | 2 | 0.16 |

## 4.3 Study III

Figure 7 shows a representative set of perfusion maps obtained from a BT measurement in one of the subjects. The gray and white matter contrast is very apparent in the CBF and CBV maps, but the mean transit time, MTT, appears to be quite homogeneous in the entire brain except for regions contaminated by cerebrospinal fluid (CSF). As expected, residual contrast agent effects became apparent when analyzing the rCBF and rCBV data obtained during rest (1st injection) and activation (2nd injection). Linear regression analysis of CBF and CBV values in non-activated ROIs, where we assumed that both parameters did not change, demonstrated a highly significant linear correlation (Table 5; Figure 8), but the slope of the regression curves was not equal to one (average ratio: CBF2/CBF1 = 1.63; CBV2/ CBV1 = 0.87). We corrected the residual bolus effects by normalizing the second CBF and CBV values to the values obtained with the first bolus injection on a pixel-by-pixel basis.

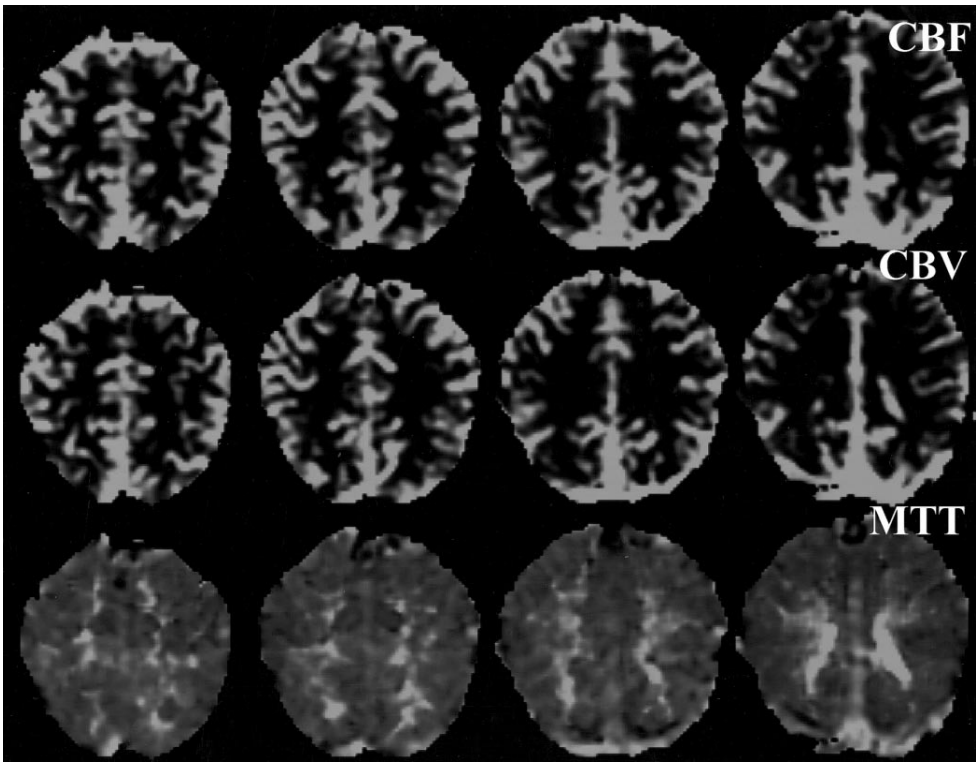


**Figure 7**. A representative set of rCBF, rCBV, and rMTT maps measured with BT. Grey/white matter differences are evident in the rCBF and rCBV images, whereas rMTT maps are quite homogeneous in the entire brain except for regions contaminated by CSF.

**Table 5**. Linear regression results for uncorrected BT rCBF and rCBV values (in nonactivated tissue) obtained during activation and the control period in eight subjects. The ratio (a), intercept (b), and Pearson product–moment coefficient (*r*) between the first and second measurements.

| | $CBF_2/CBF_1$ | | | $CBV_2/CBV_1$ | | |
|---|---|---|---|---|---|---|
| | a | b | r | a | b | r |
| Mean | 1,62 | 1.9 | 0,97 | 0,87 | 0,5 | 0,93 |
| SD | 0,84 | 3,9 | 0,04 | 0,26 | 0,52 | 0,08 |

With simultaneous motor and visual stimulation, activation in the primary sensorimotor cortex (M1), supplementary motor area (SMA), and primary visual cortex (V1) were observed in all subjects (Fig. 9). There was generally good agreement in activation responses between BOLD, FAIR, and BT measurements; however, there are observable differences in terms of the spatial extent of activation. The activation volumes detected by BOLD and FAIR are quite comparable in size, but BOLD and FAIR measurements only partially overlap. The data were calculated for pixels activated in both BOLD and FAIR measurements and should be relatively free from large vessel contribution because of the macrovascular suppression of the FAIR measurements. The average rCBV and rCBF values in the motor cortex increased by 19.4± 2.7 and 35.1 ± 8.6% respectively. The corresponding rCBV and rCBF changes in the visual cortex were 18.2 ± 2.8 and 36.9 ± 8.8% respectively. The percentage BOLD signal changes in motor and visual cortexes were 1.8 ± 0.5% and 2.6 ± 0.5% , respectively. Both BOLD and FAIR results are consistent with the data from previous studies using similar experimental conditions (Kwong *et al.,* 1992; Kim and Ugurbil, 1997; Kastrup *et al.,* 1999; Davis *et al.,* 1998)

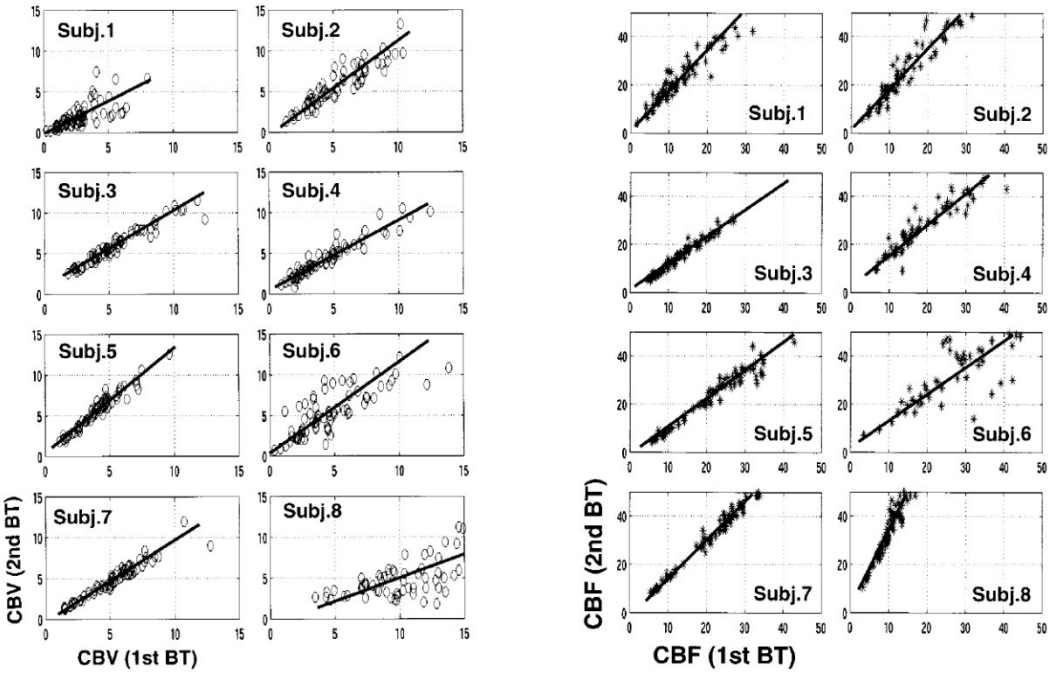


**Figure 8.** Correlation between rCBV and rCBF values from nonactivated ROIs obtained in two successive BT measurements (resting versus activation).

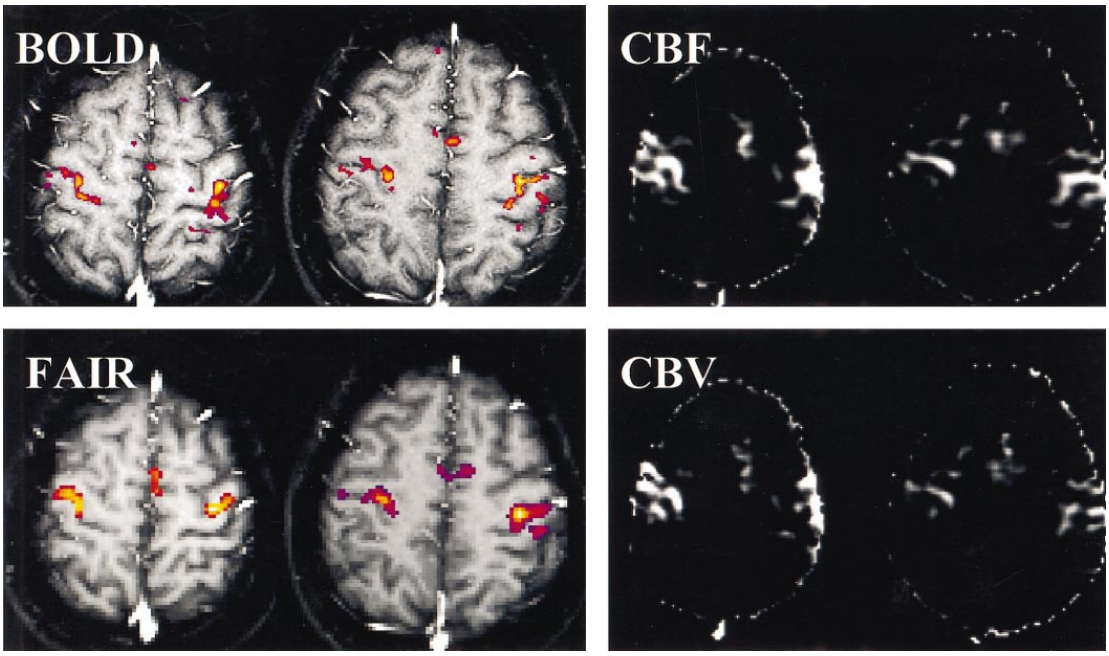


**Figure 9**. A representative set of functional activation maps for axial slices that cover the motor cortex. The identified activation by BOLD and FAIR measurements was overlaid onto the corresponding anatomic images. The bolus tracking results (CBF and CBV) are simply presented as subtracted images between resting and activation states.

## 4.4 Study IV

### 4.4.1 Scanner stability

Three measurements with a phantom were done throughout the study to control for scanner instabilities. The scans lasted for 50 minutes and an EPI sequence was used. After base line drift correction and other common pre-processing procedures, the global signal variation measured in the phantom is less than 0.3% over 50 minutes, indicating that the contribution from hardware instability of the scanner to the global signal change is nearly negligible. When comparing this with the human scans, the variation of the global signal is two orders of magnitude higher.

### 4.4.2 Physiological correction

A sub-group containing 19 subjects underwent 4 different levels of physiological corrections. The results are summarized in table 6.

**Table 6**: The average effects (N=19) of different levels of physiological noise corrections on the cross-correlation coefficients, power spectra, and associated brain network.

| Physiological noise correction steps | CC with Global signal | CC with CSF time course | Normalized Power | Volume (ml) |
|---|---|---|---|---|
| No correction | 1.00±0.00 | 0.70±0.11 | 1.00±0.63 | 420 |
| RETROICOR | 0.94±0.05 | 0.76±0.10 | 0.87±0.58 | 365 |
| Cardiac rate, RVT | 0.81±0.08 | 0.64±0.12 | 0.86±0.56 | 342 |
| Cardiac rate, RVT, CSF | 0.53±0.09 | 0.00±0.00 | 0.47±0.46 | 145 |
| CSF | 0.54±0.09 | 0.00±0.12 | 0.48±0.30 | 146 |

As shown, with more elaborated physiological noise correction, the residual power of the global signal spectrum was further reduced. Correcting the cardiac and respiration-related instabilities reduces the power by 13-14%, whereas the removal of CSF contamination reduces the power by more than 50%. Similarly, with more elaborated physiological correction, the cross-correlation coefficients of the global signal time course for the corrected resting-state fMRI datasets with the uncorrected global signal are also more markedly reduced. The CSF contribution to the global signal is also clearly manifested by the cross-correlation coefficient between the global signal and the CSF time course. Correcting the cardiac and respiratory instability has little effect on the cross-correlation coefficient between the global signal and the CSF time course, whereas regression analysis with CSF time course as regressor completely depletes the cross-correlation coefficient.
With no correction, the global signal correlates with a third of the total brain volume, but when correcting for cardiac and respiratory instabilities a reduction of 15 % of the associated brain volume is seen. When correcting for the CSF signal the associated brain volume is reduced by a factor of 3. This is illustrated in figure 10.

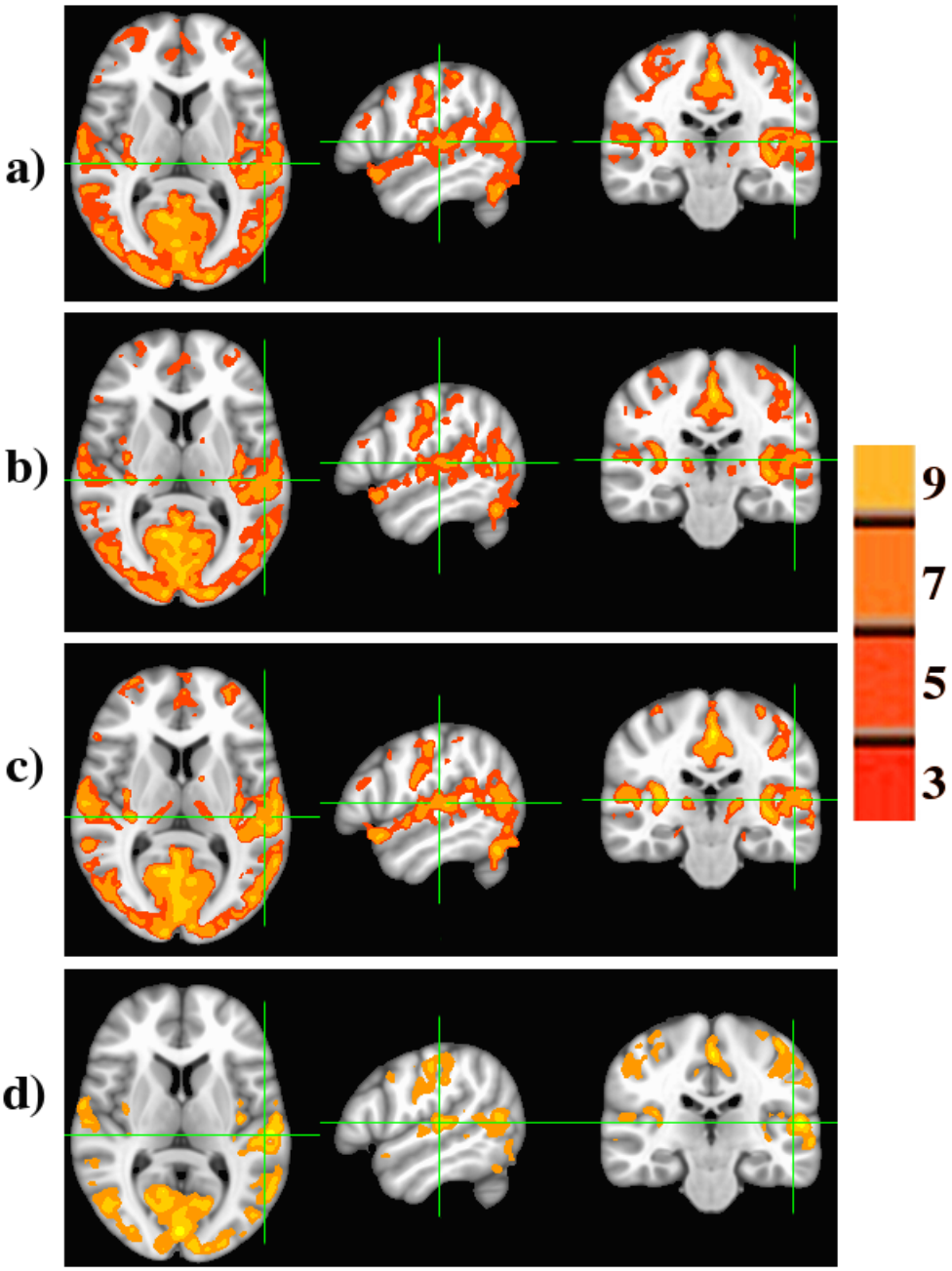


**Figure 10.** Brain regions significantly correlated with the global signal time course. Average results for resting-state fMRI data acquired from 19 normal subjects with auxilary physiological data are shown. Each row corresponds to the result for different levels of physiological noise correction. (a) Standard preprocessing, (b) Conventional RETROICOR correction; (c) Regression analysis with alignment parameters, cardiac rate, and RVT time courses as regressors; (d) Regression analysis with alignment parameters, cardiac rate, RVT, and CSF time course as regressors.

### 4.4.3 Global signal network

For the 71 subjects without physiological recordings, only motion correction parameters and the CSF signal was regressed out from the global signal. The associated brain volumes after regression were in very good agreement with the associated brain volumes in figure 10 d, which confirms that CSF is a major source of contribution to the global signal. When comparing the associated brain volumes to the global signal with standard pre-processing and with the extended regression analysis, a third of the associated brain volumes remained. These regions are listed in table 7. A consistent brain network associated with and responsible for the global signal changes in resting-state fMRI is identified. The inter-subject averaged CC map involves a number of brain regions include: posterior cingulate cortex (PCC), precuneus, inferior, middle, and superior temporal gyri, insula, medial frontal gyrus (MFG), pre- and post-central gyri, and the cerebellar vermis.

**Table 7**: The clusters of brain regions which significantly correlated with the global signal time course ($p < 0.01$, cluster size $\geq 40$ voxels) for resting-state fMRI data sets (n=108) which underwent standard preprocessing procedure and regression analysis with the alignment parameters and the CSF time course as the regressors.

| Brain region | Broadman areas | Vol (voxel) | TT Corrdinate (mm) (X, | Y, | Z) | CC | SD | MAX |
|---|---|---|---|---|---|---|---|---|
| R Posterior cingulate, precuneus | 18, 23, 30 | 122053 | -7.6 | 63.0 | 17.6 | 0.44 | 0.03 | 0.58 |
| L Postcentral gyrus, inferior parietal lobule | 2, 3, 40 | 19761 | 48.8 | 24.4 | 32.9 | 0.43 | 0.02 | 0.54 |
| R Middle and superior temporal gyri | 21, 22, 42 | 976 | -57.1 | 39.4 | 5.0 | 0.42 | 0.03 | 0.47 |
| Left Middle frontal, precentral gyri | 4, 6 | 708 | 33.5 | 7.0 | 58.0 | 0.42 | 0.03 | 0.46 |
| R Middle frontal, precentral gyri | 6 | 613 | -29.7 | 5.6 | 57.6 | 0.42 | 0.01 | 0.45 |
| L Insula | 13 | 565 | 38.3 | 15.0 | 10.8 | 0.43 | 0.02 | 0.50 |
| R Inferior and middle frontal gyri | 6, 9 | 417 | -53.2 | -11.3 | 29.8 | 0.41 | 0.02 | 0.43 |
| L Middle frontal, precentral gyri | 6, 8, 9 | 387 | 49.7 | -4.4 | 42.0 | 0.41 | 0.02 | 0.43 |
| L Middle, superior temporal gyri | 21, 22, 38 | 221 | 56.2 | -9.1 | -11.3 | 0.43 | 0.03 | 0.47 |
| R Cingulate gyrus, aracentral lobule | 6,7, 31 | 185 | -9.8 | 27.2 | 42.2 | 0.43 | 0.01 | 0.45 |
| L Insula, superior temporal gyrus | 13, 21, 22 | 127 | 38.2 | 4.4 | -5.6 | 0.41 | 0.02 | 0.43 |
| R Culmen, fusiform gyrus | 20, 36, 37 | 54 | -27.2 | 40.1 | -19.6 | 0.41 | 0.01 | 0.42 |
| R Middle and suprior temporal gyri | 22, 21, 37 | 52 | -58.2 | 55.1 | 7.9 | 0.40 | 0.01 | 0.41 |
| L Middle frontal, precentral gyri | 6 | 52 | 42.0 | 0.5 | 57.2 | 0.41 | 0.01 | 0.44 |
| L Insula | 13, 44 | 46 | 37.5 | 3.5 | 7.8 | 0.41 | 0.01 | 0.42 |

# 5 Discussion

## 5.1 Study I

In study I, two separate image registration strategies are presented. As the results shows, SigReg performs slightly better than the SepReg strategy, in terms of increased number of activated voxels and reduced standard deviation of the average $T_2$*. It is easy to realize that a separated registration for the two echoes can never match perfectly between the two echo times. The contrast is much lower for the first echo than the second echo, and the image registration algorithm will perform differently on the two data sets. Since the time between the two echoes, $\Delta$TE, is 70 ms, any head motion in this time interval will be negligible when comparing with the repetition time of 3 seconds. Even if a small difference in performance for the two different strategies is present, both methods detect the bilateral activation in the right primary motor cortex, which was not detected in the non-registered data set.

Using the number of detected activated voxels to quantitatively evaluate the image registration improvement can be unreliable, especially when it is compared with the non-registered datasets. If only random motions are dominant in the images, image registration should reduce the effective noise level and therefore increase the number of detected activated voxels. On the other hand, if stimulus-correlated motions are approximately synchronized with the stimulus changes the head motions will appear as falsely detected brain activation usually around boundaries with high signal contrast, like the brain parenchyma and the CSF, or at air/tissue boundaries. In this case, the non-registered data set might detect a higher number of activated voxels than the registered data sets. In a robust and well-known stimulus like the one used here, the finger tapping paradigm, motion induced brain activation can easily be identified and removed from further analysis, but for more complex, higher cognitive fMRI experiments, where the knowledge of the expected activated areas in the brain is vague, motion correction is mandatory.

In a study from 2001, where different image registration strategies for single shot multi echo EPI were also evaluated, a slightly different result was reported. According the study, the echo with the highest signal-to-noise ratio was always performing better than the echoes with the higher contrast in the image (Speck and Hennig, 2001). The differences might be explained by the different registration techniques used. In the later study, a 3D registration algorithm from the SPM99 package was used, while we used a 2D registration algorithm from the AFNI package. Unfortunately, we never did motion correction on the first echo and applied the motion correction parameters to the second echo, which would have been a proper comparison. More recently, a motion correction method with linear regression based on the first echo has also been proposed (Buur et al., 2009).

## 5.2 Study II

It is highly desirable to develop fMRI techniques capable of quantification and comparison between different studies. However, the BOLD signal based on $T_2$*-weighted imaging at a single TE is poorly characterized despite considerable effort using modeling and experimental approaches (Yablonskiy and Haacke, 1994, Boxerman et al., 1995, Davis et al., 1998, Li et al., 2000). Its relationship with physiological parameters such as CBF, CBV, and oxygenation level is further complicated by its dependence on acquisition parameters such as TE, TR, flip angles and sequence designs. The feasibility of quantifying BOLD signal changes is further hampered by inter-subject and within-subject variability. In order to better characterize the BOLD contrast mechanism and the spatial localization of functional signal changes during neuronal activation, acquisition techniques based on multiple time points of $R_2$* relaxation decay have been developed (Glover et al., 1996, Gati et al., 1997, Jonsson et al., 1999, Posse et al., 1999). Such techniques have the potential to distinguish $R_2$* relaxation from other factors (e.g. inflow) and to produce functional contrast less dependent on acquisition parameters. This can facilitate studies involving comparisons between exams and subjects. Another aspect is that a parameter map is insensitive to linear drifts in the signal caused by scanner electronic instabilities.

The calculation of the parameter map assumes that the signal from the voxels has a mono-exponential decay. Since the voxel volume is rather large, a mixture of different tissues, capillaries and large vessels, all with different $T_2$* values, contribute to the total voxel signal. Our results should represent the average value of vessels and tissue. Not only the $T_2$* value is dependent of the contents of the voxel. Large draining veins give a much stronger BOLD signal compared to brain parenchyma, creating a $T_2$* difference which can span over one order of magnitude(1.6-10.8 ms) (Gati et al., 1997). Even if the single shot multi echo imaging techniques use quite low resolution they provide a fast tool to obtain reliable $T_2$* distributions in the human brain when compared to $T_2$* mapping with a FLASH sequence(Klarhofer et al., 2002). When Bandettini et al used a combination of gradient-echo and spin-echo data, they found that spin-echo was insensitive to large vessels. Using only voxels that were activated in both methods(Bandettini et al., 1994) they found a $T_2$* difference of 1.3 ms between activation and rest, which can be compared to the result in this thesis, 3.6 ms and 4.7 ms for Study I and Study II, respectively. In a comparable study, which also used a single shot multi-echo sequence but a 2 T MRI scanner, a $\Delta T_2$* = 3.6 ms was seen, and this is in good agreement with our observation if the differences in activation paradigm and magnetic field strength are taken into account (Speck and Hennig, 1998). In study I and study II, two echoes at different echo times were used to map $T_2$* by assuming a mono-exponential decay. Acquiring more echoes as in other studies (Barth et al., 1999, Posse et al., 1999) might produce a more robust fitting of the relaxation decay curve. Multiple echo data acquisition can also be useful for detecting a non mono exponential

relaxation decay phenomena which has been previously reported in a $T_2$ study of gray matter(Whittall et al., 1999).

$T_2$* mapping allows quantitative comparison of activation-induced $\Delta T_2$* across subjects and studies. However, $T_2$*-mapping does not necessarily generate the highest functional sensitivity. As can be seen in study II, the activated volume detected by $T_2$* mapping is significantly less than that for $T_2$*-weighted imaging at $TE_2$ = 90 ms, even though the sensitivity for $T_2$* weighted imaging has not yet been optimized at TE = 90 ms. One explanation for this can be that the SNR is deteriorated when calculating the $T_2$* maps which is not compensated for. The CNR is practically identical for the $T_2$* maps and for the second echo $T_2$*-weighted images, which is surprising, since CNR is assumed to be a good measure for functional sensitivity, and the difference in activated voxels is 40% between the two data sets. There is a significant correlation between CNR and detected activated voxels, but the correlation is rather weak (r=0.39). A possible explanation for this is that the CNR values calculated using SNR values determined outside the activation areas do not reflect the noise level difference in the activation areas.

Single-shot multi-echo sequences can be useful in other ways than for calculating the activated voxels in the $T_2$* map. Glover et al used a dual-echo spiral in/spiral out sequence to reduce signal losses in the frontal lobes and to increase the sensitivity(Glover and Law, 2001), while Weiskopf et al used an alternating phase encoding gradient for the consecutive echoes in a multi-echo sequence, to reduce image distortions (Weiskopf et al., 2005). One can also use the $T_2$* map to optimize the BOLD contrast for the $T_2$*-weighted images, since the optimal TE is approximately the $T_2$* value. It has been shown that the $T_2$* value varies strongly across the brain and between subjects (Hagberg et al., 2002). Combining $T_2$* maps and parallel imaging acquisition Poser et al developed a inhomogenity-desensitized fMRI method which optimized pixelwise weighted echo summation based on local $T_2$* measurements (Poser et al., 2006). Recently, single-shot multi-echo EPI has also been used in resting-state fMRI to differentiate between BOLD and non-BOLD signals (Kundu et al., 2011). This indicates that multi-echo fMRI can be very useful for characterizing some important aspects of the BOLD signal.

## 5.3 Study III

Only a few human fMRI studies have investigated changes in the rCBV during functional activation prior to this work (Belliveau et al., 1991, Zigun et al., 1993, Frank et al., 1994). These studies used BT measurements but assumed that the signal intensity-time profile of the second bolus injection was not influenced by the first bolus injection. This assumption was later found to be incorrect, since the effect of residual contrast agent can be seen hours after injection (Levin et al., 1995). In study III, the residual contrast effect on the second BT measurement was corrected assuming that

CBV (and CBF) do not change in non-activated brain areas between the two bolus injections. The correction involved two steps: First, it was established that there is a good linear correlation between the data sets from the two successive BT measurements in non-activated regions. Using the value obtained for the slope of the regression curve, the CBF and CBV data were then corrected from the second BT measurement to match the values obtained with the first BT measurement. When comparing the measured rCBV and the calculated rCBV using Grubbs law, a marked difference was seen. The estimated rCBV data was consistently lower than the measured rCBV data, implying that Grubb's law may underestimate the rCBV based on measured rCBF values. These results indicate that caution must be applied when using the above stated power-law relationship to estimate rCBV changes during functional activation in humans. One explanation of the difference can be that the Grubb relationship is based on a hypercapnia-based CBF modulation on anesthetized primates. Not only is it difficult to translate results from animals to humans, the CBF regulatory mechanisms for hypercapnia and neuronal activation are likely to be different. Secondly, the relationship between CBF and CBV may change due to changes in cerebral metabolism, which occur at neuronal activation but not with hypercapnia. The Grubb relationship has been used frequently to estimate the oxygen metabolism change ($\Delta CMRO_2$) using calibrated BOLD techniques (Hoge et al., 1999, Kastrup et al., 2002, Chiarelli et al., 2007). The exact form of this relationship is now under debate, since several studies have come up to other constants in the power-law relationship using PET (Ito et al., 2001, Ito et al., 2003, Rostrup et al., 2005) and MRI (Chen and Pike, 2009).

The magnitude of the estimated ΔCBV from study III was 19 % in the visual cortex and 18 % in the motor cortex. These values are somewhat lower than what was reported in other studies; 24 % (Mandeville et al., 1998), 27 % (Francis et al., 2003) and 32 % (Belliveau et al., 1991, Gu et al., 2006). Newly developed non-invasive MRI techniques have also been used to determine the ΔCBV during neuronal activation: a study based on vascular space occupancy, VASO, sequence reported a ΔCBV of 56 % (Lu and van Zijl, 2005), which is substantially higher than the result from study III, while another study using a pulse sequence sensitive to only the venous CBV, VERVE (venous refocusing for volume estimation), produced a much lower values, between 10-14 % (Chen and Pike, 2009). The latter study might be more relevant for BOLD response, since the BOLD contrast is established in the venous side of the capillaries.

Our rCBF values are in good agreement with results from earlier studies e g (Li et al., 1999a, Li et al., 1999b), but the ranges reported can vary between 30-100%. Despite the high absolute magnitude of the CBF changes, the low contrast-to-noise ratios in the perfusion based methods require considerable signal averaging to detect robust CBF changes. With multimodality fMRI measurements including BOLD, FAIR, and bolus tracking of contrast agent, rCBF, rCBV and BOLD signal change can be determined and the contribution of hemodynamic and oxidative metabolic parameters to BOLD signal changes can be assessed quantitatively.

## 5.4 Study IV

The results of study IV demonstrate that a significant portion of the global signal time course is likely to be linked to neural activity. About 50% of the variance in the global signal could be explained by fluctuations in physiological instabilities related to cardiac rate, respiration, and CSF motions. Earlier studies have stated that the global signal is mainly of non-neuronal origin and recommend removing the contribution of the global signal from the resting-state fMRI data (Hampson et al., 2002, Birn et al., 2006, Chang and Glover, 2009a) to enhance the quality of the observations of the brain's intrinsic, large-scale functional architecture (Fox et al., 2005, Weissenbacher et al., 2009, Van Dijk et al., 2010). This has been questioned, especially because of the effect it might have on the anti-correlations observed between different functional networks. In particular, the interpretation of the default mode network ( see review on DMN (Buckner et al., 2008)) becomes a very relevant issue (Raichle et al., 2001, Fransson, 2005) considering its involvement with the anti-correlation phenomena and the global signal removal. Resting-state fMRI time course of the default-mode network is thought to be negatively correlated with that of the "task-positive network", a collection of regions commonly recruited in demanding cognitive tasks. However, most resting-state fMRI studies have employed some form of global signal normalization and such processing steps alter the time courses of voxels giving rise to spurious negative correlations (Cole et al., 2010). The apparent negative correlations in many of the task-positive regions could be artificially induced by pre-processing procedures, such as, physiological noise correction and global signal removal (Murphy et al., 2009). It has been shown that physiological noise correction increased the spatial extent and magnitude of negative correlations and caused region-specific decreases in positive correlations within the default-mode network. Although it may still be appropriate to remove the global component in order to focus on the differences in local correlation strength, growing evidence in the literature (Leopold et al., 2003, He et al., 2008, Hyder and Rothman, 2010, Schölvinck et al., 2010, Chen, 2011) and the results of study IV indicate that a substantial portion of the global time course is very likely to be linked to underlying neural activity, and the result inferred from the removal of the global signal must therefore be interpreted with caution. Other regressors than the global signal have been proposed to remove signals which are unlikely to have neuronal origin, such as CSF, white matter and other non-brain tissue (Behzadi et al., 2007, Bianciardi et al., 2009, Giove et al., 2009, Anderson et al., 2010)

Local field potentials, LFP, studies in primate (Leopold et al., 2003, Schölvinck et al., 2010) showed that a considerable portion of the variance in global fMRI signal is related to the slow modulation of neuronal events represented by the high- and low-frequency LFP bands. However, it is not certain to what extent the spontaneous fluctuations of the global signal are coupled with the baseline neuronal activity. The power spectrum of the global signal time course indicates that physiological instability may contribute to about 50% of the variance energy. $^{13}C$ magnetic resonance spectroscopy (MRS) studies aimed at brain energy consumption can give us further clues on this. $^{13}C$ MRS studies in rats have established that about 80% of the neuronal energy in the cerebral cortex supports the global neuronal activity at rest (Hyder and Rothman, 2010). If this also applies to the human brain, it can explain why the global

signal changes measured in fMRI are much higher than that of the task-invoked local BOLD signal.

The remaining portion of the global signal originates from a consistent brain network covering approximately 150 ml brain volume. The power spectrum of the global signal time course differs individually, but most of its energy is distributed in the low frequency range <0.04 Hz. Since the global signal network shows inter-subject consistency it is reasonable to hypothesize that the global network is related to the perception and cognitive processes of the brain that occur during a resting-state fMRI experiment. These may include inward thinking about the subject itself, thought suppression, the effort to keep the body still in a relaxed position, sensing the spatial orientation of lying in the gantry, and adaptation of the hearing to the noisy environment due to rapidly switching gradients. Most of these sensory perceptions, cognition and control processes can actually be explained by the functions of the brain regions associated with the global signal network. It is known that PCC is activated in situations when a person is inwardly oriented, in unconscious problem solving and in daydreaming. Cerebellar vermis is the termination site of spinocerebellar pathways that carry out unconscious proprioception and is linked to the brain's natural ability to integrate and analyze inertial motion. Purkinje cells in this area are thought to receive sensory information from the vestibular system of the inner ears and use this to compute information about the body's orientation in space. The superior temporal gyrus (STG) is involved in hearing. Classical neuropsychology findings suggest that the right STG subserves nonverbal sound discrimination, recognition, and comprehension. Prefrontal cortex, cingulate, and insula are known to be involved with conscious thought suppression. At present, it is not clear to us why these different brain regions with distinct functions generate coherent activities during resting-state fMRI scans. The suppressions of thought and body movement are probably modulated similarly by the sensory input from the scanning environments.

The neurophysiological basis of the BOLD fMRI signal has been extensively studied, particularly in the context of invoked response to a stimulus. Studies of tasked-based and resting-state fMRI have revealed that BOLD fMRI signal changes are tightly linked to neural activity. On the other hand, there is growing consensus that the relationship between the BOLD fMRI signal and the underlying neural activity is complex and numerous physiological factors, including even behavioral state, contribute to the modulation of microvasculature. This implies that explicating the neurophysiological basis for baseline global signal changes is quite challenging because there is lack of well defined timing, event, and reference status for comparison. However, determining the purpose and consequences of intrinsic activities may prove to be of high importance for understanding the brain’s most fundamental physiological principles. As discussed above, converging evidence suggest that spontaneous intrinsic events including the global signal changes, as opposed to sensory processing or motor execution, accounts for the majority of the brain’s large energy consumption. It is quite intriguing to consider that synchronous global signal changes in an inter-subject consistent brain network contribute significantly to the energy consumption but has no essential functionality. It is natural then to ask: What drives these intrinsic neural fluctuations in the brain and do such fluctuations optimize the functionality of the cortex?

# Acknowledgements

I would like to thank the following people who have contributed to my PhD and who are important to me:

First of all, a special thanks to my main supervisor **Tie-Qiang Li**, for always being there for me during this 13 years' long road to a PhD. Without you, I would never have finished my work. Thank you also for the good times we have had outside work, both here and abroad, you have become a good friend to me.

Thanks to my two co-supervisors; **Peter Aspelin**, for always supporting me when I came with problems and questions, even when my PhD seemed to be far, far away, **Anders Wennerberg**, for recruiting me to Huddinge and helping me during the first time here. Too bad you moved away for other challenges.

My boss**, Leif Svensson**, thank you for giving me time for my research projects, even if you claim that research and development is written in my work description, not everyone thinks that way.

**Hans Forssberg**, thank you for introducing me to the research field and having me as a PhD student my first years.

My co-workers at the MR Unit at Medical Physics, **Love** and **Martin**, thanks for making my days fun and interesting, and believe it or not, meaningful, the few times you learn something from me.

Thanks to **Eva Ö**, for reviewing my thesis, for being my permanent lunch-buddy and for our efforts to solve network problems at ImageLab.

**Helena Forssell,** thanks for reading through and commenting my thesis, and helping me with all the KI stuff that I needed help with.

**Susanne M** and **Maria K-W**, thanks for letting me play with your MRI-scanners, and for our constructive modus operandi, it's always fun to work with you.

All my **co-workers at the medical physics department in Huddinge, physicists, nurses and the admin staff**, for the friendly and jokey climate at our department, sometimes it feels like it's always Friday!

**All the staff at the MR unit in Huddinge,** it is always fun and easy to work with you guys, and I look forward to increase my presence at the unit, more than I have been lately, not only because of your nice "fikabröd".

To all my **friends in my O-club**, thanks for the good times we have had on our training camps, competition travels and Palmis' well-organized annual spring training trip. Being out in the woods is like a battery charger for me, where I gather strength and harmony for the working days.

Thanks also to the **members of OIT** for making your best to humiliate me at our annual meetings.

**Jonas P**, thank you for our late movie nights in combination with beer and deep philosophical discussions, I wish I remembered the conclusions better…

My big brother **Stefan**, thank you for being my best friend and for always helping and inspiring me, I hope we will have more time to do things together in the future.

My parents, **Kenneth and Gunvor**, thank you for being the best parents you can wish for, always believing in me and letting me try my wings on my own, and taking care of me if the wings didn't carry.

To my wife **Annelie**, thank you for being in my life and supporting my work. I love the thought of growing old with you. And **Elina**, our daughter, she reminds me daily of what life really is about, curiosity, development, responsibility and lots and lots of love.

# 6 References


Anderson JS, Druzgal TJ, Lopez-Larson M, Jeong EK, Desai K, Yurgelun-Todd D (2010) Network anticorrelations, global regression, and phase-shifted soft tissue correction. Hum Brain Mapp.

Bandettini PA, Wong EC, Hinks RS, Tikofsky RS, Hyde JS (1992) Time course EPI of human brain function during task activation. Magn Reson Med 25:390-397.

Bandettini PA, Wong EC, Jesmanowicz A, Hinks RS, Hyde JS (1994) Spin-echo and gradient-echo EPI of human brain activation using BOLD contrast: a comparative study at 1.5 T. NMR Biomed 7:12-20.

Barth M, Metzler A, Klarhofer M, Roll S, Moser E, Leibfritz D (1999) Functional MRI of the human motor cortex using single-shot, multiple gradient-echo spiral imaging. Magn Reson Imaging 17:1239-1243.

Beckmann CF, DeLuca M, Devlin JT, Smith SM (2005) Investigations into resting-state connectivity using independent component analysis. Philos Trans R Soc Lond B Biol Sci 360:1001-1013.

Behzadi Y, Restom K, Liau J, Liu TT (2007) A component based noise correction method (CompCor) for BOLD and perfusion based fMRI. Neuroimage 37:90-101.

Belliveau JW, Kennedy DN, Jr., McKinstry RC, Buchbinder BR, Weisskoff RM, Cohen MS, Vevea JM, Brady TJ, Rosen BR (1991) Functional mapping of the human visual cortex by magnetic resonance imaging. Science 254:716-719.

Bianciardi M, van Gelderen P, Duyn JH, Fukunaga M, de Zwart JA (2009) Making the most of fMRI at 7 T by suppressing spontaneous signal fluctuations. Neuroimage 44:448-454.

Birn RM, Diamond JB, Smith MA, Bandettini PA (2006) Separating respiratory-variation-related fluctuations from neuronal-activity-related fluctuations in fMRI. Neuroimage 31:1536-1548.

Birn RM, Murphy K, Bandettini PA (2008) The effect of respiration variations on independent component analysis results of resting state functional connectivity. Hum Brain Mapp 29:740-750.

Biswal B, Yetkin FZ, Haughton VM, Hyde JS (1995) Functional connectivity in the motor cortex of resting human brain using echo-planar MRI. Magn Reson Med 34:537-541.

Biswal BB, Mennes M, Zuo XN, Gohel S, Kelly C, Smith SM, Beckmann CF, Adelstein JS, Buckner RL, Colcombe S, Dogonowski AM, Ernst M, Fair D, Hampson M, Hoptman MJ, Hyde JS, Kiviniemi VJ, Kotter R, Li SJ, Lin CP, Lowe MJ, Mackay C, Madden DJ, Madsen KH, Margulies DS, Mayberg HS, McMahon K, Monk CS, Mostofsky SH, Nagel BJ, Pekar JJ, Peltier SJ, Petersen SE, Riedl V, Rombouts SA, Rypma B, Schlaggar BL, Schmidt S, Seidler RD, Siegle GJ, Sorg C, Teng GJ, Veijola J, Villringer A, Walter M, Wang L, Weng XC, Whitfield-Gabrieli S, Williamson P, Windischberger C, Zang YF, Zhang HY, Castellanos FX, Milham MP (2010) Toward discovery science of human brain function. Proc Natl Acad Sci U S A 107:4734-4739.

Bloch F, Hansen WW, Packard M (1946) The nuclear induction experiment. Physical Review 70:474-485.

Boxerman JL, Hamberg LM, Rosen BR, Weisskoff RM (1995) MR contrast due to intravascular magnetic susceptibility perturbations. Magn Reson Med 34:555-566.

Buckner RL, Andrews-Hanna JR, Schacter DL (2008) The brain's default network: anatomy, function, and relevance to disease. Ann N Y Acad Sci 1124:1-38.

Buur PF, Poser BA, Norris DG (2009) A dual echo approach to removing motion artefacts in fMRI time series. Nmr in Biomedicine 22:551-560.

Buxton RB, Wong EC, Frank LR (1998) Dynamics of blood flow and oxygenation changes during brain activation: the balloon model. Magn Reson Med 39:855-864.

Chang C, Cunningham JP, Glover GH (2009) Influence of heart rate on the BOLD signal: the cardiac response function. Neuroimage 44:857-869.
Chang C, Glover GH (2009a) Effects of model-based physiological noise correction on default mode network anti-correlations and correlations. Neuroimage 47:1448-1459.
Chang C, Glover GH (2009b) Relationship between respiration, end-tidal CO2, and BOLD signals in resting-state fMRI. Neuroimage 47:1381-1393.
Chen G (2011) Characterize the distribution and behavior significance of the global signal measured by resting-state functional connectivity in elderly. In: ISMRM, p 2193 Montreal: Wiley.
Chen JJ, Pike GB (2009) BOLD-specific cerebral blood volume and blood flow changes during neuronal activation in humans. NMR Biomed 22:1054-1062.
Chiarelli PA, Bulte DP, Gallichan D, Piechnik SK, Wise R, Jezzard P (2007) Flow-metabolism coupling in human visual, motor, and supplementary motor areas assessed by magnetic resonance imaging. Magn Reson Med 57:538-547.
Cole DM, Smith SM, Beckmann CF (2010) Advances and pitfalls in the analysis and interpretation of resting-state FMRI data. Front Syst Neurosci 4:8.
Cox RW (1996) AFNI: software for analysis and visualization of functional magnetic resonance neuroimages. Comput Biomed Res 29:162-173.
Damoiseaux JS, Rombouts SA, Barkhof F, Scheltens P, Stam CJ, Smith SM, Beckmann CF (2006) Consistent resting-state networks across healthy subjects. Proc Natl Acad Sci U S A 103:13848-13853.
Davis TL, Kwong KK, Weisskoff RM, Rosen BR (1998) Calibrated functional MRI: mapping the dynamics of oxidative metabolism. Proc Natl Acad Sci U S A 95:1834-1839.
de Zwart JA, Gelderen P, Fukunaga M, Duyn JH (2008) Reducing correlated noise in fMRI data. Magn Reson Med 59:939-945.
Detre JA, Leigh JS, Williams DS, Koretsky AP (1992) Perfusion imaging. Magn Reson Med 23:37-45.
Ernst T, Hennig J (1994) Observation of a fast response in functional MR. Magn Reson Med 32:146-149.
Fox MD, Snyder AZ, Vincent JL, Corbetta M, Van Essen DC, Raichle ME (2005) The human brain is intrinsically organized into dynamic, anticorrelated functional networks. Proc Natl Acad Sci U S A 102:9673-9678.
Fox MD, Zhang D, Snyder AZ, Raichle ME (2009) The global signal and observed anticorrelated resting state brain networks. J Neurophysiol 101:3270-3283.
Francis ST, Pears JA, Butterworth S, Bowtell RW, Gowland PA (2003) Measuring the change in CBV upon cortical activation with high temporal resolution using look-locker EPI and Gd-DTPA. Magn Reson Med 50:483-492.
Frank JA, Mattay VS, Duyn J, Sobering G, Barrios FA, Zigun J, Sexton R, Kwok P, Woo J, Moonen C, et al. (1994) Measurement of relative cerebral blood volume changes with visual stimulation by 'double-dose' gadopentetate-dimeglumine-enhanced dynamic magnetic resonance imaging. Invest Radiol 29 Suppl 2:S157-160.
Fransson P (2005) Spontaneous low-frequency BOLD signal fluctuations: an fMRI investigation of the resting-state default mode of brain function hypothesis. Hum Brain Mapp 26:15-29.
Gati JS, Menon RS, Ugurbil K, Rutt BK (1997) Experimental determination of the BOLD field strength dependence in vessels and tissue. Magn Reson Med 38:296-302.
Giove F, Gili T, Iacovella V, Macaluso E, Maraviglia B (2009) Images-based suppression of unwanted global signals in resting-state functional connectivity studies. Magn Reson Imaging 27:1058-1064.
Glover GH, Law CS (2001) Spiral-in/out BOLD fMRI for increased SNR and reduced susceptibility artifacts. Magn Reson Med 46:515-522.
Glover GH, Lemieux SK, Drangova M, Pauly JM (1996) Decomposition of inflow and blood oxygen level-dependent (BOLD) effects with dual-echo spiral gradient-recalled echo (GRE) fMRI. Magn Reson Med 35:299-308.

Glover GH, Li TQ, Ress D (2000) Image-based method for retrospective correction of physiological motion effects in fMRI: RETROICOR. Magn Reson Med 44:162-167.
Gu H, Lu H, Ye FQ, Stein EA, Yang Y (2006) Noninvasive quantification of cerebral blood volume in humans during functional activation. Neuroimage 30:377-387.
Hagberg GE, Indovina I, Sanes JN, Posse S (2002) Real-time quantification of T(2)(*) changes using multiecho planar imaging and numerical methods. Magn Reson Med 48:877-882.
Hampson M, Peterson BS, Skudlarski P, Gatenby JC, Gore JC (2002) Detection of functional connectivity using temporal correlations in MR images. Hum Brain Mapp 15:247-262.
He BJ, Snyder AZ, Zempel JM, Smyth MD, Raichle ME (2008) Electrophysiological correlates of the brain's intrinsic large-scale functional architecture. Proc Natl Acad Sci U S A 105:16039-16044.
Hoge RD, Atkinson J, Gill B, Crelier GR, Marrett S, Pike GB (1999) Investigation of BOLD signal dependence on cerebral blood flow and oxygen consumption: the deoxyhemoglobin dilution model. Magn Reson Med 42:849-863.
Hu X, Le TH, Parrish T, Erhard P (1995) Retrospective estimation and correction of physiological fluctuation in functional MRI. Magn Reson Med 34:201-212.
Hyder F, Rothman DL (2010) Neuronal correlate of BOLD signal fluctuations at rest: err on the side of the baseline. Proc Natl Acad Sci U S A 107:10773-10774.
Ito H, Kanno I, Ibaraki M, Hatazawa J, Miura S (2003) Changes in human cerebral blood flow and cerebral blood volume during hypercapnia and hypocapnia measured by positron emission tomography. J Cereb Blood Flow Metab 23:665-670.
Ito H, Takahashi K, Hatazawa J, Kim SG, Kanno I (2001) Changes in human regional cerebral blood flow and cerebral blood volume during visual stimulation measured by positron emission tomography. J Cereb Blood Flow Metab 21:608-612.
Jansma JM, Ramsey NF, Slagter HA, Kahn RS (2001) Functional anatomical correlates of controlled and automatic processing. J Cogn Neurosci 13:730-743.
Jonsson T (1997) The effect of voxel size and echo time in functional mri. In: Department of medical radiation physics, vol. MSc, p 28 Stockholm: Karolinska institutet, Stockholm university.
Jonsson T, Wennerberg AB, Forssberg H, Glover GH, Li TQ (1999) An image registration strategy for multi-echo fMRI. J Magn Reson Imaging 10:154-158.
Kastrup A, Kruger G, Neumann-Haefelin T, Glover GH, Moseley ME (2002) Changes of cerebral blood flow, oxygenation, and oxidative metabolism during graded motor activation. Neuroimage 15:74-82.
Klarhofer M, Barth M, Moser E (2002) Comparison of multi-echo spiral and echo planar imaging in functional MRI. Magn Reson Imaging 20:359-364.
Kruger G, Glover GH (2001) Physiological noise in oxygenation-sensitive magnetic resonance imaging. Magn Reson Med 46:631-637.
Kruger G, Kastrup A, Glover GH (2001) Neuroimaging at 1.5 T and 3.0 T: comparison of oxygenation-sensitive magnetic resonance imaging. Magn Reson Med 45:595-604.
Kundu P, Inati SJ, Evans JW, Luh W-M, Bandettini PA (2011) Differentiating BOLD and Non-BOLD Signals in fMRI Time Series Using Multi-Echo EPI. NeuroImage.
Kwong KK, Belliveau JW, Chesler DA, Goldberg IE, Weisskoff RM, Poncelet BP, Kennedy DN, Hoppel BE, Cohen MS, Turner R, et al. (1992) Dynamic magnetic resonance imaging of human brain activity during primary sensory stimulation. Proc Natl Acad Sci U S A 89:5675-5679.
Leopold DA, Murayama Y, Logothetis NK (2003) Very slow activity fluctuations in monkey visual cortex: implications for functional brain imaging. Cereb Cortex 13:422-433.
Levin JM, Kaufman MJ, Ross MH, Mendelson JH, Maas LC, Cohen BM, Renshaw PF (1995) Sequential dynamic susceptibility contrast MR experiments in human brain: residual contrast agent effect, steady state, and hemodynamic perturbation. Magn Reson Med 34:655-663.

Li TQ, Haefelin TN, Chan B, Kastrup A, Jonsson T, Glover GH, Moseley ME (2000) Assessment of hemodynamic response during focal neural activity in human using bolus tracking, arterial spin labeling and BOLD techniques. Neuroimage 12:442-451.

Li TQ, Kastrup A, Takahashi AM, Moseley ME (1999a) Functional MRI of human brain during breath holding by BOLD and FAIR techniques. Neuroimage 9:243-249.

Li TQ, Moseley ME, Glover G (1999b) A FAIR study of motor cortex activation under normo- and hypercapnia induced by breath challenge. Neuroimage 10:562-569.

Li TQ, Takahashi A, Wang Y, Mathews V, Glover GH (2006) Dual-echo spiral in/in acquisition method for reducing magnetic susceptibility artifacts in blood-oxygen-level-dependent functional magnetic resonance imaging. Magnetic Resonance in Medicine 55:325-334.

Ljunggren S (1983) A simple graphical representation of Fourier based imaging methods. J Magn Reson 54:338-343.

Lu H, van Zijl PC (2005) Experimental measurement of extravascular parenchymal BOLD effects and tissue oxygen extraction fractions using multi-echo VASO fMRI at 1.5 and 3.0 T. Magn Reson Med 53:808-816.

Mandeville JB, Marota JJ, Kosofsky BE, Keltner JR, Weissleder R, Rosen BR, Weisskoff RM (1998) Dynamic functional imaging of relative cerebral blood volume during rat forepaw stimulation. Magn Reson Med 39:615-624.

Menon RS, Ogawa S, Hu X, Strupp JP, Anderson P, Ugurbil K (1995) BOLD based functional MRI at 4 Tesla includes a capillary bed contribution: echo-planar imaging correlates with previous optical imaging using intrinsic signals. Magn Reson Med 33:453-459.

Murphy K, Birn RM, Handwerker DA, Jones TB, Bandettini PA (2009) The impact of global signal regression on resting state correlations: are anti-correlated networks introduced? Neuroimage 44:893-905.

Ogawa S, Lee TM, Kay AR, Tank DW (1990) Brain magnetic resonance imaging with contrast dependent on blood oxygenation. Proc Natl Acad Sci U S A 87:9868-9872.

Ogawa S, Tank DW, Menon R, Ellermann JM, Kim SG, Merkle H, Ugurbil K (1992) Intrinsic signal changes accompanying sensory stimulation: functional brain mapping with magnetic resonance imaging. Proc Natl Acad Sci U S A 89:5951-5955.

Ostergaard L, Sorensen AG, Kwong KK, Weisskoff RM, Gyldensted C, Rosen BR (1996a) High resolution measurement of cerebral blood flow using intravascular tracer bolus passages. Part II: Experimental comparison and preliminary results. Magn Reson Med 36:726-736.

Ostergaard L, Weisskoff RM, Chesler DA, Gyldensted C, Rosen BR (1996b) High resolution measurement of cerebral blood flow using intravascular tracer bolus passages. Part I: Mathematical approach and statistical analysis. Magn Reson Med 36:715-725.

Pauling L, Coryell CD (1936) The Magnetic Properties and Structure of Hemoglobin, Oxyhemoglobin and Carbonmonoxyhemoglobin. Proc Natl Acad Sci U S A 22:210-216.

Poser BA, Versluis MJ, Hoogduin JM, Norris DG (2006) BOLD contrast sensitivity enhancement and artifact reduction with multiecho EPI: Parallel-acquired inhomogeneity-desensitized fMRI. Magnetic Resonance in Medicine 55:1227-1235.

Posse S, Wiese S, Gembris D, Mathiak K, Kessler C, Grosse-Ruyken ML, Elghahwagi B, Richards T, Dager SR, Kiselev VG (1999) Enhancement of BOLD-contrast sensitivity by single-shot multi-echo functional MR imaging. Magn Reson Med 42:87-97.

Purcell EM, Torrey HC, Pound RV (1946) Resonance Absorption by Nuclear Magnetic Moments in a Solid. Physical Review 69:37.

Raichle ME, MacLeod AM, Snyder AZ, Powers WJ, Gusnard DA, Shulman GL (2001) A default mode of brain function. Proc Natl Acad Sci U S A 98:676-682.

Rostrup E, Knudsen GM, Law I, Holm S, Larsson HB, Paulson OB (2005) The relationship between cerebral blood flow and volume in humans. Neuroimage 24:1-11.
Schölvinck ML, Maier A, Ye FQ, Duyn JH, Leopold DA (2010) Neural basis of global resting-state fMRI activity. Proc Natl Acad Sci U S A 107:10238-10243.
Shmueli K, van Gelderen P, de Zwart JA, Horovitz SG, Fukunaga M, Jansma JM, Duyn JH (2007) Low-frequency fluctuations in the cardiac rate as a source of variance in the resting-state fMRI BOLD signal. Neuroimage 38:306-320.
Speck O, Hennig J (1998) Functional imaging by I0- and T2*-parameter mapping using multi-image EPI. Magn Reson Med 40:243-248.
Speck O, Hennig J (2001) Motion correction of parametric fMRI data from multi-slice single-shot multi-echo acquisitions. Magnetic Resonance in Medicine 46:1023-1027.
Triantafyllou C, Hoge RD, Krueger G, Wiggins CJ, Potthast A, Wiggins GC, Wald LL (2005) Comparison of physiological noise at 1.5 T, 3 T and 7 T and optimization of fMRI acquisition parameters. Neuroimage 26:243-250.
Twieg DB (1983) The k-trajectory formulation of the NMR imaging process with applications in analysis and synthesis of imaging methods. Med Phys 10:610-621.
Van Dijk KR, Hedden T, Venkataraman A, Evans KC, Lazar SW, Buckner RL (2010) Intrinsic functional connectivity as a tool for human connectomics: theory, properties, and optimization. J Neurophysiol 103:297-321.
van Houdt PJ, Ossenblok PP, Boon PA, Leijten FS, Velis DN, Stam CJ, de Munck JC (2010) Correction for pulse height variability reduces physiological noise in functional MRI when studying spontaneous brain activity. Hum Brain Mapp 31:311-325.
Weiskopf N, Klose U, Birbaumer N, Mathiak K (2005) Single-shot compensation of image distortions and BOLD contrast optimization using multi-echo EPI for real-time fMRI. Neuroimage 24:1068-1079.
Weissenbacher A, Kasess C, Gerstl F, Lanzenberger R, Moser E, Windischberger C (2009) Correlations and anticorrelations in resting-state functional connectivity MRI: a quantitative comparison of preprocessing strategies. Neuroimage 47:1408-1416.
Whittall KP, MacKay AL, Li DK (1999) Are mono-exponential fits to a few echoes sufficient to determine T2 relaxation for in vivo human brain? Magn Reson Med 41:1255-1257.
Wise RG, Ide K, Poulin MJ, Tracey I (2004) Resting fluctuations in arterial carbon dioxide induce significant low frequency variations in BOLD signal. Neuroimage 21:1652-1664.
Yablonskiy DA, Haacke EM (1994) Theory of NMR signal behavior in magnetically inhomogeneous tissues: the static dephasing regime. Magn Reson Med 32:749-763.
Zigun JR, Frank JA, Barrios FA, Jones DW, Foo TK, Moonen CT, Press DZ, Weinberger DR (1993) Measurement of brain activity with bolus administration of contrast agent and gradient-echo MR imaging. Radiology 186:353-356.
Öberg J, Jonsson T, Li TQ (2011) Aging related changes in functional connectivity networks investigated by resting-state BOLD functional MRI: A study of independent compartment analysis and image preprocessing procedures. Submitted.